Magnetostratigraphy of Pliocene sediments from the Stirone River (Po Valley)

C. Mary, S Iaccarino, V. Courtillot, J Besse ', D M Aissaoui

Geophys. J. Int. (1993) **112**, 359–380

Magnetostratigraphy of Pliocene sediments from the Stirone River (Po Valley)

C. Mary,[1] S. Iaccarino,[2] V. Courtillot,[1] J. Besse[1] and D. M. Aissaoui[3]

[1] *Laboratoire de Paléomagnétisme et de Géodynamique, Institut de Physique du Globe de Paris, 4 Place Jussieu, F-75252 Paris 05, France*
[2] *Istituto di Geologia, Università di Parma, 43100 Parma, Italy*
[3] *Département de Géologie, CNRS-UA 723, Université Paris Sud, F-91405 Orsay, France*

Accepted 1992 July 15. Received 1991 November 15; in original form 1991 February 25

SUMMARY

The Miocene–Pliocene and Pliocene–Pleistocene boundaries bracket a Pliocene section, approximately 800 m thick, along the Stirone river near Parma (Northern Italy). From the base to the top, the sequence consists mainly of blue clays (Zanclean in age), whitish laminates, silty clays and sandstones of Piacenzian age. A debris flow, which is the sedimentary expression of a hiatus, separates the Zanclean from the Piacenzian sediments. Thermomagnetic analysis, thermal evolution of magnetic susceptibility, acquisition and removal of anhysteretic and isothermal remanent magnetization (ARM and IRM) by alternating field and thermal methods, X-ray diffraction and scanning electron-microscopy (SEM) have been used in conjunction to try and unravel the complex magnetic mineralogy of the Stirone samples. Two major carriers of the magnetic remanence appear to be pseudo-single domain (PSD) magnetite and high-coercivity pyrrhotite in varying amounts and grain sizes. Five different magnetic indicators yield roughly consistent logs, with magnetite being important in the lower part of the section and pyrrhotite becoming dominant upsection. Six zones with more or less uniform properties have been outlined. Except in the lowermost zone where magnetite is also an important carrier, pyrrhotite in the 150–350 °C range is taken to be the main carrier of the characteristic and, we believe, primary magnetization. The overall mean direction for about 200 samples is $D = 0°$, $I = 52°$ ($\alpha_{95} = 3°$), corresponding to a lack of local rotation about a vertical axis but implying some 10° of inclination shallowing. The magnetostratigraphy encompasses ten successive polarity zones. Correlation of magnetic and biostratigraphic results to the geomagnetic polarity time scale and to the biozonation of the Mediterranean area leads to the proposal that the Thvera subchron and part of the above reversed polarity zone are missing, as revealed by the absence of the *Sphaeroidinellopsis seminulina* s.l. Zone and by the occurence of *Globorotalia margaritae* from the very base of the section. The Sidufjall and Nunivak subchrons are recognized and the first occurrence of *Globorotalia puncticulata* occurs just above Nunivak subchron. The Cochiti subchron is observed next. A remarkable hiatus involves the upper part of the Gilbert chron up to the lower part of the Kaena subchron based on the record of the last occurrence of *G. margaritae* and *G. puncticulata* and the first occurence of *G. aemiliana* and *G. bononiensis*. Another hiatus involving the Reunion and Olduvai subchrons is suggested to occur in the upper part of the Pliocene sequence based on the absence of the *G. inflata* Zone and on the first occurrence of *Artica islandica,* which marks the Pliocene/Pleistocene boundary, towards the top of the section. The average sedimentation rate is estimated to be 450–500 m Ma^{-1} for the early Pliocene and 200–300 m Ma^{-1} for the late Pliocene. Despite highly non-uniform sedimentation, both reflecting the episodic nature of coupled tectonic and sedimentary processes on

the Appenine–Po flexure and events of larger geographical extent, the section compares favourably with other Italian Pliocene magnetostratigraphies.

Key words: Italy, magnetostratigraphy, natural ion sulphides, Pliocene.

INTRODUCTION

The only way in which biostratigraphic events can be compared and calibrated on a worldwide basis is through unambiguous correlation with well identified magnetic reversals. Up to now magnetostratigraphy has been applied with this aim in mind to the late Neogene of the Mediterranean area only for short sections of Pliocene and Pleistocene stratigraphic intervals. Most of these biomagnetostratigraphic studies concern land sections in Crete, Rhodos (Lovlie, Stole & Spjeldnaes 1989) and Southern Italy (Tauxe *et al.* 1983; Zijderveld *et al.* 1986; Channell, Rio & Thunell 1988; Zachariasse *et al.* 1989) and cores in the Tyrrhenian Sea (Leg 107) (Channell *et al.* 1990) and in Central Italy (Arias *et al.* 1990).

According to the most recent data, the Miocene–Pliocene boundary (MPB), defined at the Capo Rossello section in Sicily (Cita 1975), falls below the Thvera subchron (Arias *et al.* 1980; Tauxe *et al.* 1983; Zijderveld *et al.* 1986; Zachariasse *et al.* 1989); it has been recalibrated by Hilgen & Langereis (1988) at 4.86 Ma. However, at the type section and elsewhere in Sicily, the Upper Miocene magnetostratigraphy is actually missing, preventing precise correlation of this boundary with sediments from outside the Mediterranean area. The Pliocene–Pleistocene boundary (PPB), recently defined at Vrica in Southern Italy (Colalongo *et al.* 1982; Aguirre & Pasini 1985; Bassett 1985; Pasini, Colalongo & Sartoni 1992), occurs just above the Olduvai subchron (Bucha *et al.* 1975; Nakagawa 1977; Arias *et al.* 1980; Tauxe *et al.* 1983; Aïfa, Feinberg & Pozzi 1988; Lovlie, Stole & Spjeldnaes 1989). Yet, the faunas found in Italy depend to a large extent on their palaeoenvironment and significant diachronism has been demonstrated (Colalongo *et al.* 1972, 1984; Hills & Thierstein 1989).

Many tributaries flowing down from the Appenines into the Po River in Northern Italy offer interesting sections for biomagnetostratigraphic study of Pliocene and Pleistocene marine sediments. Nakagawa (1977) published a magnetostratigraphy from one of these tributaries, the Santerno River, but the results are very difficult to interpret. Tric *et al.* (1991) have recently presented a detailed analysis of the Olduvai polarity transition in another tributary, the Crostolo River (Pelosio & Raffi 1973). The present study is based on a section in the Stirone River and offers a first

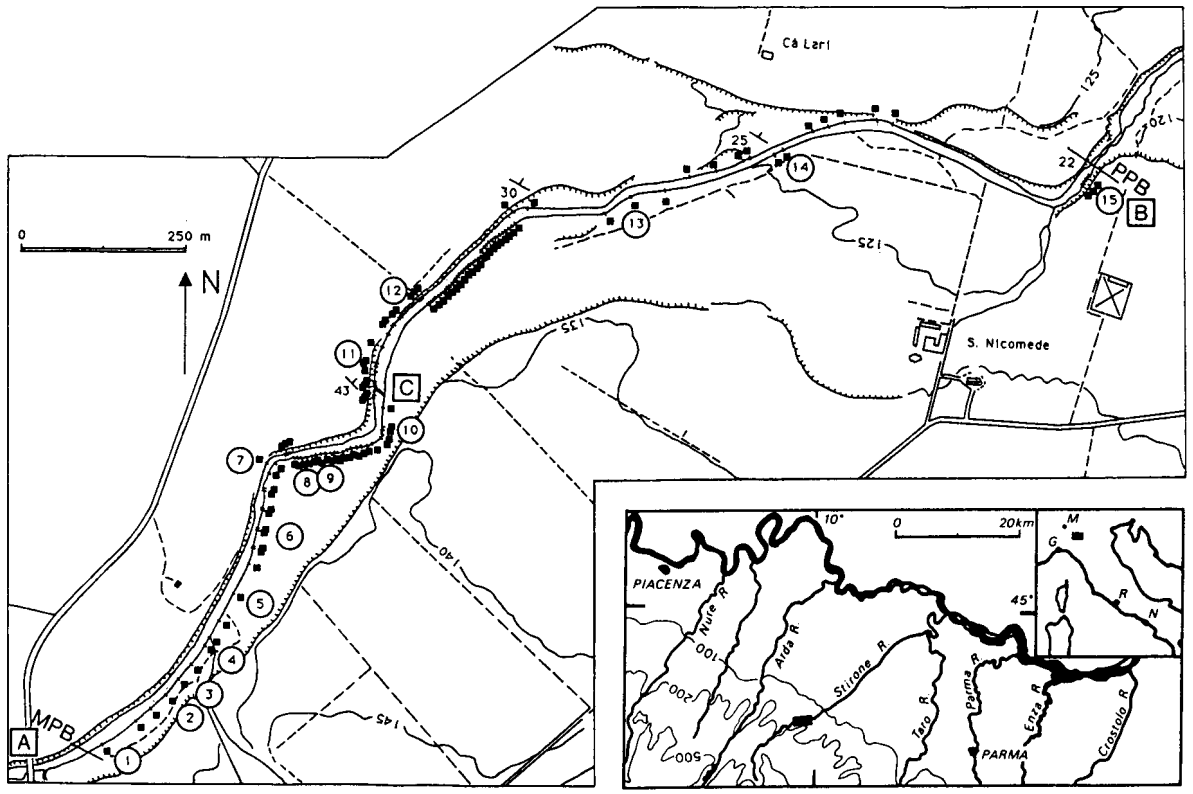

Figure 1. Geographical location of the Stirone River (a) and sampling sites in Pliocene sediments along the river (squares in b). Circled numbers (1 to 15) correspond to 'test' samples discussed in the mineralogical study; MPB: Mio–Pliocene Boundary; PPB: Plio–Pleistocene Boundary. A: Ponte Scipione; B: San Nicomede calcarenite level; C: isolated calcarenite bed forming a convenient reference.

attempt of correlation of the Plio–Pleistocene datum levels with the reversal time scale in Northern Italy.

The Stirone River (Fig. 1a) merges with the Taro River not far from Parma. Because of very active erosion, the section is well exposed along the river banks. The section we investigated is located near Salsomaggiore Terme, a few kilometers away from the Tabian stratotype (Iaccarino 1967), and about 15 km from the Piacenzian stratotype (Barbieri 1967; Rio *et al.* 1988). It extends for 4 km from Scipione Ponte to the San Nicomede church (respectively A and B in Fig. 1b). It straddles 60 m of lago–mare Messinian sediments (Iaccarino & Papani 1979) and about 800 m of Pliocene sediments up to the PPB. The section continues upwards with Pleistocene sediments.

Preliminary magnetostratigraphic analyses (Bucha 1975; Besse & Kukla, unpublished data, 1985) concern the topmost 80 m of the Pliocene sequence and lowest 120 m of the Pleistocene sediments. We resampled the whole Pliocene sequence, with the aim of obtaining a more complete magnetostratigraphy of Pliocene and Pleistocene sediments, and correlating it with the biostratigraphic results. Previous magnetic work had demonstrated the presence of several magnetic minerals with a complex distribution of overlapping components. We have therefore undertaken a rather detailed chemical, physical and magnetic analysis of the sediments, which is a prerequisite to a meaningful interpretation of the palaeomagnetic directions.

LITHOLOGY AND BIOSTRATIGRAPHY

The Stirone sequence was first described by Papani & Pelosio (1962). At that time part of the present exposure was buried under fluvial deposits. Because of the active erosion in the last few years a natural waterfall, encompassing the PPB, was destroyed around 1980 and, at the time of sampling (1989–90), the sequence was almost entirely exposed from the base to the top. A simplified stratigraphic section is shown in Fig. 2(a). The MPB which occurs at the top of Messinian lago–mare marlstones (Iaccarino & Papani 1979) as in the Sicilian Capo Rossello stratotype section, represents the base of the investigated section, while the PPB represents the top.

The lower part of the section is characterized by 398 m of massive and homogeneous blue clays. The absence of evident sedimentary structures prevented an accurate measurement of bedding. Rare slump structures were observed within this interval. A calcarenitic layer ('C' in Fig. 1b), 3 m thick, interpreted as a debris flow, interrupts the clayey sedimentation. From 401 m to 416 m the sequence consists of whitish laminites, alternating with thin marly layers. From this interval upwards, the stratification is more noticeable, showing a NNE dipping trend varying from 40° to 25° and becomes progressively more horizontal in the upper part of the section. From 416 m to 600 m the sequence consists mostly of sandy clays with intercalated lenses of sandy fossiliferous and algal detritus. From 600 m to the top, the sediments show increasing shallow water features and consist of fossiliferous sands with lenticular sandstone layers. The topmost part of this interval is characterized by 20 m of beach sediments (the 'calcarenite' of Papani & Pelosio 1962). The Pleistocene sediments documented in

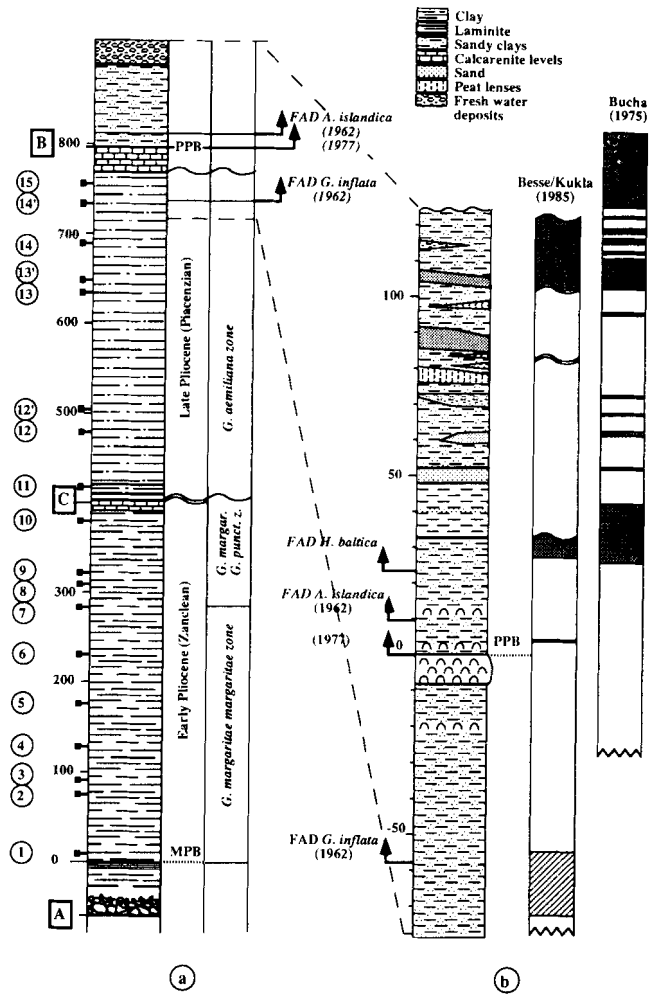

Figure 2. (a) Stratigraphic log of the Pliocene and Pleistocene sediments along the Stirone River (see text for more details). Biostratigraphic zonations from Papani & Pelosio (1962), Pelosio & Raffi (1977), Raffi (1982), Iaccarino & Pugliese (1988). (b) Enlargement of the upper part of the section, with the main biological events. Two magnetostratigraphic columns, from Bucha *et al.* (1975), and Besse & Kukla (1985, personal communication) are also shown.

great detail by Pelosio & Raffi (1977) are representative of an infralittoral environment with intercalations of brackish and fresh water episodes (peat lenses, paleosoils, . . .); they extend upwards for more than 100 m.

The foraminifera and molluscs, as well as ostracods and pollen of the Stirone Plio–Pleisotcene sequence have been described by various authors (Papani & Pelosio 1962; Pelosio & Raffi 1977; Bertolani Marchetti *et al.* 1979; Iaccarino & Papani 1979, 1982; Raffi 1982; Iaccarino & Pugliese 1988; Capotondi *et al.* 1992; Iaccarino *et al.* 1992).

In Fig. 2(a), the planktonic foraminifera biozones recognized in the Stirone sequence following the zonal scheme of Iaccarino (1985) are plotted. By comparison with the Pliocene biozones, it appears that the *Sphaeroidinellopsis seminulina* s.l., *Globorotalia puncticulata* and *Globorotalia inflata* Zones are missing. This last zone was documented by Papani & Pelosio (1962) but was definitely no more recognized by Iaccarino *et al.* (1993)

despite the strong erosion of the river bed. The absence of these biozones corresponds to three major biostratigraphic hiatuses. The lowest hiatus involves the basal Zanclean; the second one, the lowermost Piacenzian (between the blue clays and the 'C' calcarenite in Figs 1 and 2); the third hiatus involves the late Piacenzian.

The PPB, defined by the FO of *A. islandica*, occurs just on the topmost layer of the thick calcarenite which marks the top of the investigated section (Pelosio & Raffi 1977). In 1962, Papani & Pelosio first found this FO 10 m higher. This event, known to be one of the most reliable (Pelosio, Raffi & Rio 1979; Raffi 1986) virtually coincides with the FO of *C. testudo* which has been adopted for the PPB (Colalongo & Pasini 1980; Colalongo, Pasini & Sartoni 1980; Colalongo *et al.* 1982; Aguirre & Pasini 1985). *Geophyrocapsa oceanica*, the calcareous nannofossil whose FO approximates the PPB as defined at the Vrica type section (Colalongo *et al.*; Backman, Shackleton & Tauxe 1983) appears higher in the Stirone section (Raffi 1982; Rio, Backman & Raffi 1992), and *Hyalinea baltica*, whose FO is estimated at 1.4 Ma, first occurs still higher (Pelosio & Raffi 1977). Palynological data of the late Pliocene and Pleistocene Stirone sequence (Bertolani Marchetti *et al.* 1979) indicate climatic variations, following a cold period centred on the PPB.

MAGNETIC MINERALOGY

(a) Sampling

Samples were taken along the entire Pliocene outcrop, with a maximum spacing between the sites of 15 m; at least four samples were taken at each site. Site locations (123 sites plus 300 cores along 60 m just above sample '12') are indicated by black squares in Fig. 1(b). Only wet sediments were sampled. One inch (2.54 cm) long oriented cores were drilled whenever possible; when the sediment was found to be too soft for drilling, one inch oriented cubic samples were taken. The samples were brought back to the laboratory still wet, and then left to dry in mu-metal shields. The magnetization of some of the samples was measured at intervals during the time they dried (3–4 days) and showed a decay of the natural remanent magnetization (NRM) of 10–15 per cent with partial destruction of a viscous component.

(b) Analysis, first observations, previous work

Samples were demagnetized both in a nearly-zero-field laboratory built furnace and by alternating fields (AF) in a Schonstedt DSM1 equipment. Magnetizations were measured on a CTF three-axis SQUID magnetometer, and the evolution of susceptibility was monitored during thermal demagnetization. Acquisition and removal (by thermal or AF treatment) of anhysteretic remanent magnetization (ARM) and isothermal remanent magnetization (IRM) were also studied in order to characterize better the magnetic minerals (Linssen 1988; Channell *et al.* 1990). All experiments and measurements were undertaken in the mu-metal/steel shielded room at IPG in Paris.

Fig. 3 shows a typical example in which all these measurements were performed. This sample comes from the lower part of the section and clearly displays two main ranges of unblocking temperatures (Fig. 3b), a first one between 100 °C and 300 °C, and another one between 450 °C and ~600 °C. In each range two components can be separated (Fig. 3a). Although different types of behaviour were observed upon demagnetization, the NRM intensity of most samples had dropped by about 80 per cent after stepwise thermal cleaning up to 400 °C.

The presence of at least two distinct magnetic carriers had already been observed in many Mediterranean sediments of similar age. Authors have suggested the presence of [maghemite and magnetite or titanomagnetite, iron sulfide (pyrrhotite or greigite) and magnetite] (Tauxe *et al.* 1983; Aïfa *et al.* 1988; Lovlie *et al.* 1989; Zachariasse *et al.* 1989; Linssen 1988), but few have reported a precise mineralogical study. In some Italian sections, the NRM is carried by iron sulfides only (greigite–Tric *et al.* 1991; and pyrrhotite–Arias *et al.* 1980, Channell & Hawthorne 1990). The importance of iron sulfides is probably related to the high accumulation rates of the clays. Rapid burial of organic matter, sulfate and detrital iron minerals enhances the formation of pyrite and other iron sulfides (Berner 1983).

(c) Thermomagnetic analysis, thermal evolution of susceptibility, X-ray diffraction and SEM

We have attempted to establish which magnetic minerals were present in the Pliocene clays of the Stirone section, and to determine whether they carried the NRM or not. In order to identify these magnetic carriers, we studied in particular detail fifteen levels along the section (1 to 15, plus complimentary samples 12′, 13′ and 14′, close to 12, 13 and 14 respectively, as indicated on Figs. 1b and 2). We have tried to extract the magnetic minerals by circulating a slurry, made of the bulk sediment mixed with water, between the polar pieces of an electromagnet or close to a rare earth magnet (Channell & Hawthorne 1990). After a while, the tubing was washed with pure water, and magnetic minerals attracted by the magnet were collected. Magnetic extracts were subjected to thermomagnetic studies, Scanning Electron Microscope observations (Philips 50 SEM) and microprobe analyses (EDS link system). Thermomagnetic analyses were carried out on three samples with a vertical Curie balance. The thermomagnetic curve obtained from sample 13′ is shown in Fig. 4. Most of the saturation magnetization is lost at temperatures less than 310 °C, and the remaining magnetization disappears before 600 °C. Because saturation magnetization is much higher upon cooling than on heating in the 300 °C–550 °C range, the main magnetic mineral must have been converted to other phases, among which is magnetite. The characteristic bump around 250 °C on the cooling curve indicates the presence of antiferromagnetic Fe_9S_{10} pyrrhotite (Schwarz 1975). Hence, the mineral which disappears beyond 300 °C and converts to magnetite and pyrrhotite must be an iron sulfide. Thermomagnetic curves such as that in Fig. 4 show that 75 per cent of the saturation remanence of the unheated specimen must reside in sulfides.

Maghemite is sometimes recognized in Italian sediments (Lovlie *et al.* 1989), but the behaviour of χ_0 of our samples allows one to exclude this mineral: during stepwise heating, the susceptibilities of all samples increased after 350 °C, and

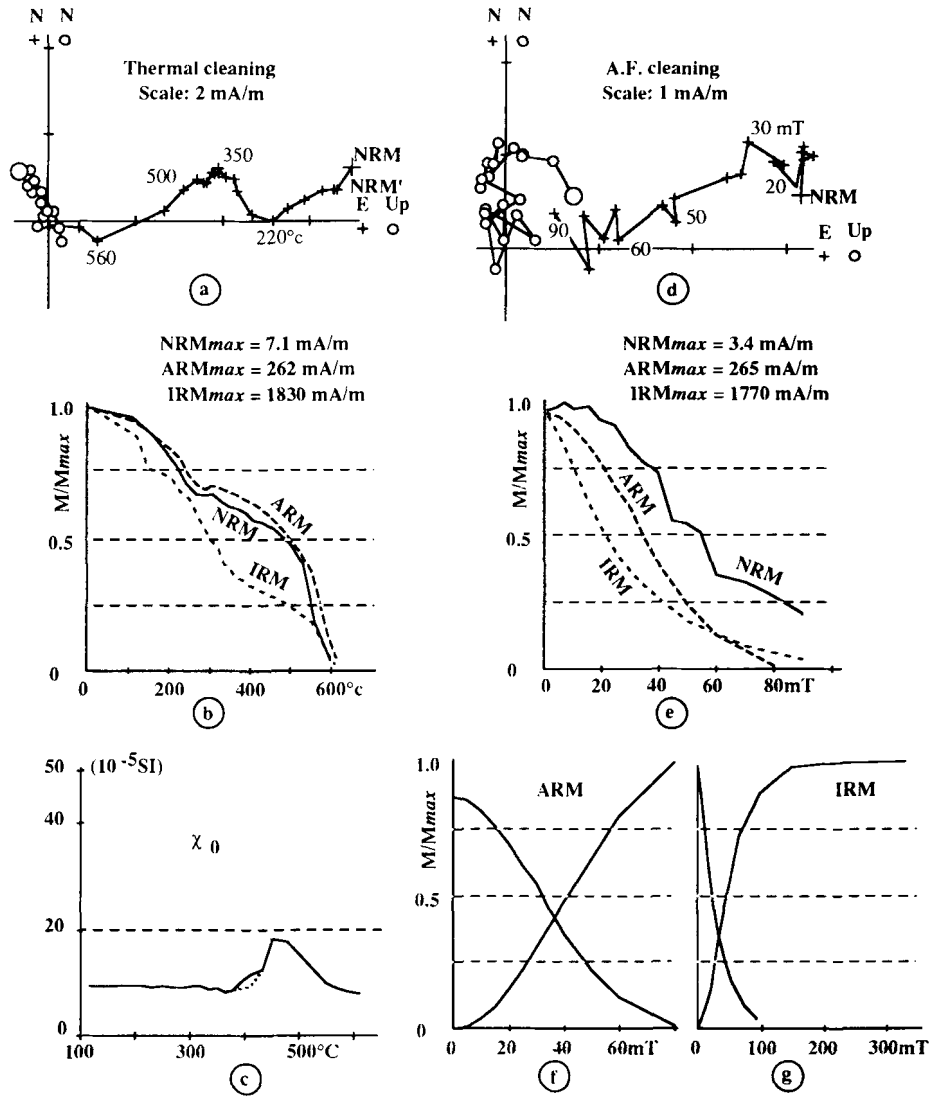

Figure 3. Synthesis of the results obtained with 'test' sample 1; for position see Figs 1 and 2; (a) [resp. (d)] vector Zijderveld diagrams (after stratigraphic correction) of demagnetization by thermal (resp. AF) treatment. Open circles and crosses indicate projections respectively on the N–S vertical plane and the horizontal plane. NRM′: magnetization after a stay in mu-metal sheilds; (b) [resp. (e)] evolution of the NRM, ARM and IRM during thermal (resp. AF) demagnetization; (c) stepwise thermal evolution of χ_0; (f) stepwise demagnetization and acquisition of ARM; (g) stepwise acquisition and demagnetization of IRM.

decreased before 600 °C (e.g. Fig. 3c). Therefore, magnetite is formed after 350 °C from a low χ_0 mineral, whereas maghemite has the same χ_0 as magnetite, and is usually converted to low χ_0 haematite by 500 °C.

X-ray diffraction experiments (using a monochromatic diffractometer $-CuK_\alpha$ radiation) allow us to identify magnetite in magnetic extracts from all samples (Fig. 5a). In some samples (such as 4 and 5), pure magnetite X-ray spectra are observed, yet thermal demagnetization clearly reveals a lower T_c component besides magnetite. For some reason, the lower T_c mineral has not been extracted from the sample in the process of preparation for X-ray analysis. Pyrite and pyrrhotite have been recognized in some of the spectra (Fig. 5b) and greigite cannot be ruled out in one sample from the Upper Pliocene (test sample 14′); on the other hand, the main characteristic peaks of maghemite never appear.

With SEM observations and microprobe analyses, framboidal pyrite and hexagonal non-magnetic pyrrhotite (Fig. 6a and b) have been found respectively in samples 14′ and 12′. Aggregates of iron sulfides that appear in sample 14′ may correspond to greigite (Fig. 6c). This is suggested by their composition, where only iron and sulphur are detectable, and by their clumsy shape contrasting with the euhedral pyrrhotite crystals. Very little iron sulfide was found in samples 4 and 5, but the magnetic extracts contain a lot of calcitic spheres with tiny magnetite crystals pasted on them (Mary 1991). In the magnetic extract from sample 4, tiny iron sulfide crystals were found inside foraminifera (Fig. 6d and e); therefore, we infer that the extracted

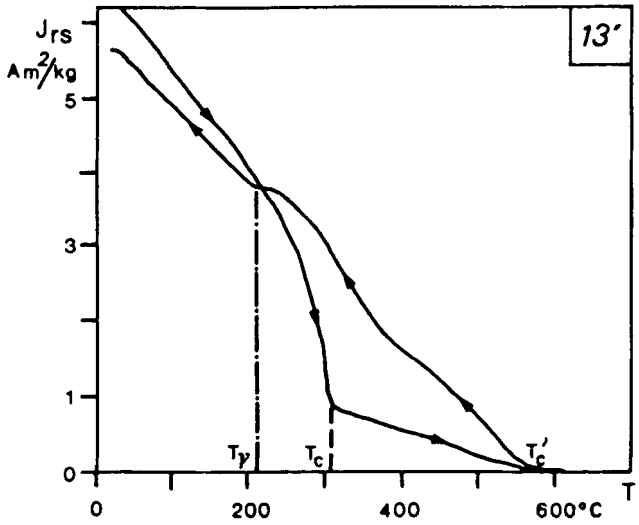

Figure 4. Thermomagnetic curve (vertical Curie balance, under vacuum) of a sample from the Upper Pliocene (close to 'test' sample '13'); Tγ: γ transition of hexagonal pyrrhotite; Tc: Curie Point of iron sulfide minerals (greigite or monoclinic pyrrhotite); Tc': Curie point of magnetite.

calcitic spheres contain the magnetic iron sulfides. No magnetic mineral could be extracted from sample 10, possibly because all the magnetic minerals at this level are contained within calcitic spheres which cannot easily be separated from the bulk sediment.

In conclusion, magnetite is a ubiquitous magnetic carrier in sediments of the Stirone section, whereas maghemite is absent. Thermomagnetic experiments, X-ray diffraction and SEM observations clearly demonstrate the presence of iron sulfides in these sediments in varying amounts. Microprobe and SEM analyses show large grain magnetite of detrital origin, mixed with titanomagnetite and splinters of a mineral containing iron and chrome, interpreted as chromite (Fig. 7a and b). Chromite is usually found in ophiolitic complexes (Nicolas 1989), and some ophiolitic blocks are observed in the Apennines close to the Stirone River. Only non-magnetic iron sulfides, that is pyrite (FeS_2) and pyrrhotite (Fe_9S_{10}), are found upon SEM observation of some samples, but thermal experiments show that magnetic sulfides are also present. These sulfides are apparently often attached to calcite spheres and/or to foraminifera and are not isolated in most magnetic extracts. These magnetic minerals must be either monoclinic pyrrhotite (Fe_7S_8) or greigite (Fe_3S_4).

(d) Acquisition and removal of ARM and IRM

The magnetic minerals identified (magnetite and pyrrhotite) in the Stirone section can be further characterized by a comparative analysis of their magnetic properties, some of which are already mentioned in the previous paragraph. The saturation remanent magnetizations of magnetite (1–20 $Am^2 kg^{-1}$; Collinson 1983) and pyrrhotite (2–6 $Am^2 kg^{-1}$; Dekkers 1988) are in the same range. The low field susceptibility of pyrrhotite is much weaker than that of magnetite (Dekkers 1988). Upon heating, pyrrhotite of all grain sizes becomes demagnetized at relatively low temperatures (compared to magnetite), i.e. below 350 °C and demagnetization occurs over a rather narrow range of

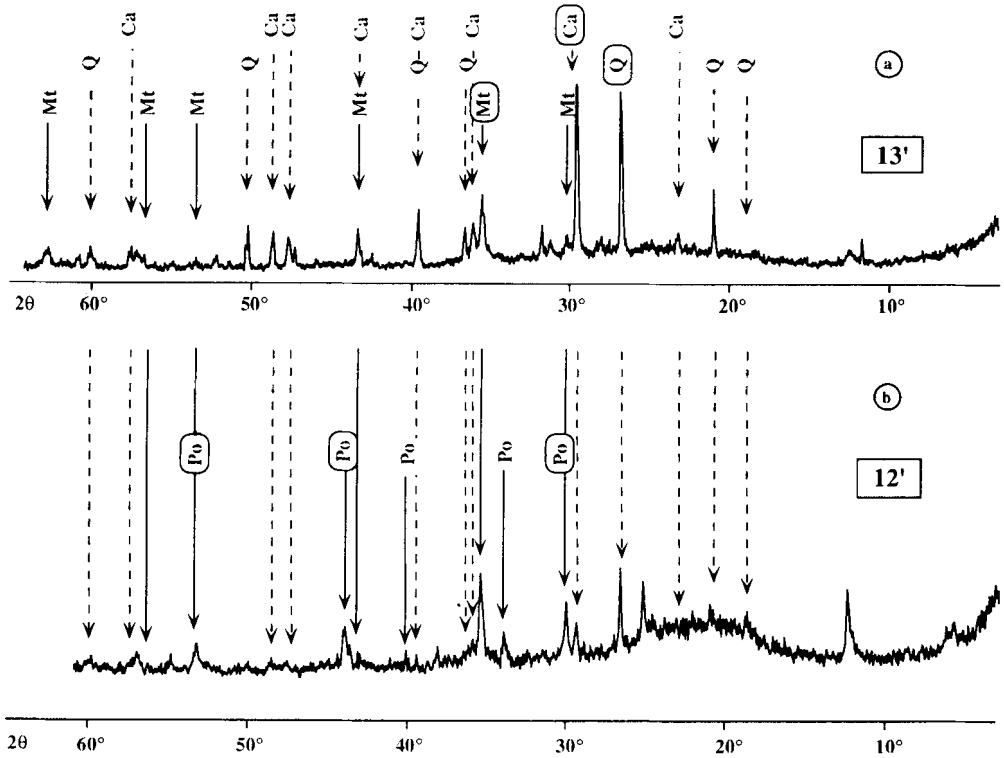

Figure 5. X-ray diffraction spectra of sample 13' (a) and 14' (b); solid arrows: spectral peaks of iron oxides or sulfides; dashed arrows: spectral peaks of non-magnetic minerals. Main peaks of each mineral are circled. Mt: magnetite; Po: pyrrhotite; Py: Pyrite; Ca: calcite; Q: quartz.

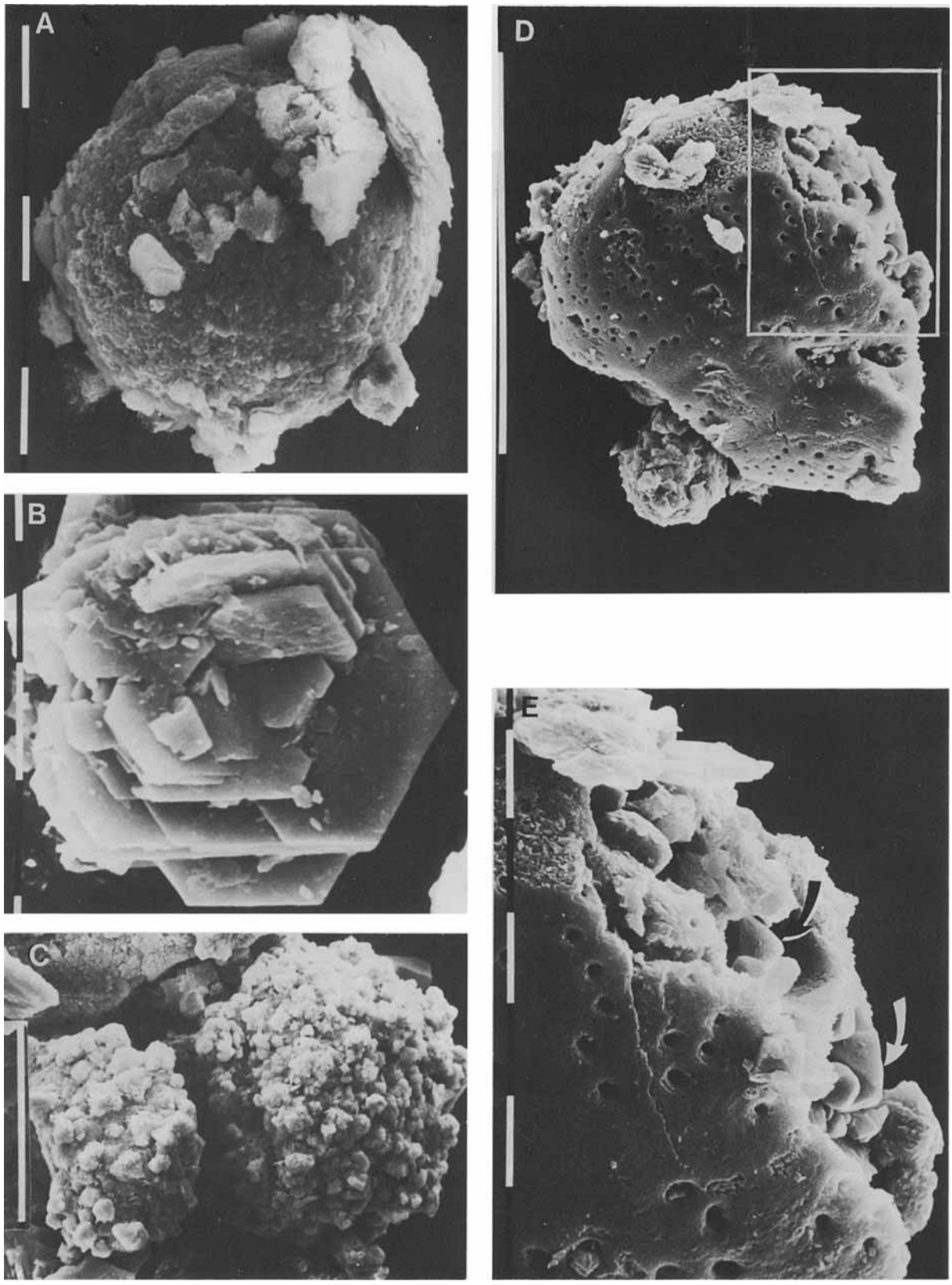

Figure 6. SEM views of iron sulfide minerals. (A) Framboidal pyrite (sample 13′; bar: 10 μm); (B) euhedral crystals of hexagonal pyrrhotite (sample 12′; bar: 10 μm); (C) cluster of iron sulfide crystal, probably greigite (sample 14′; bar: 50 μm); (D) and (E) piece of broken cell wall of a foraminifera, *Globigerina sp.* (sample 5; bars: 10 μm). The cell infilling includes iron sulfide crystals (arrows in E).

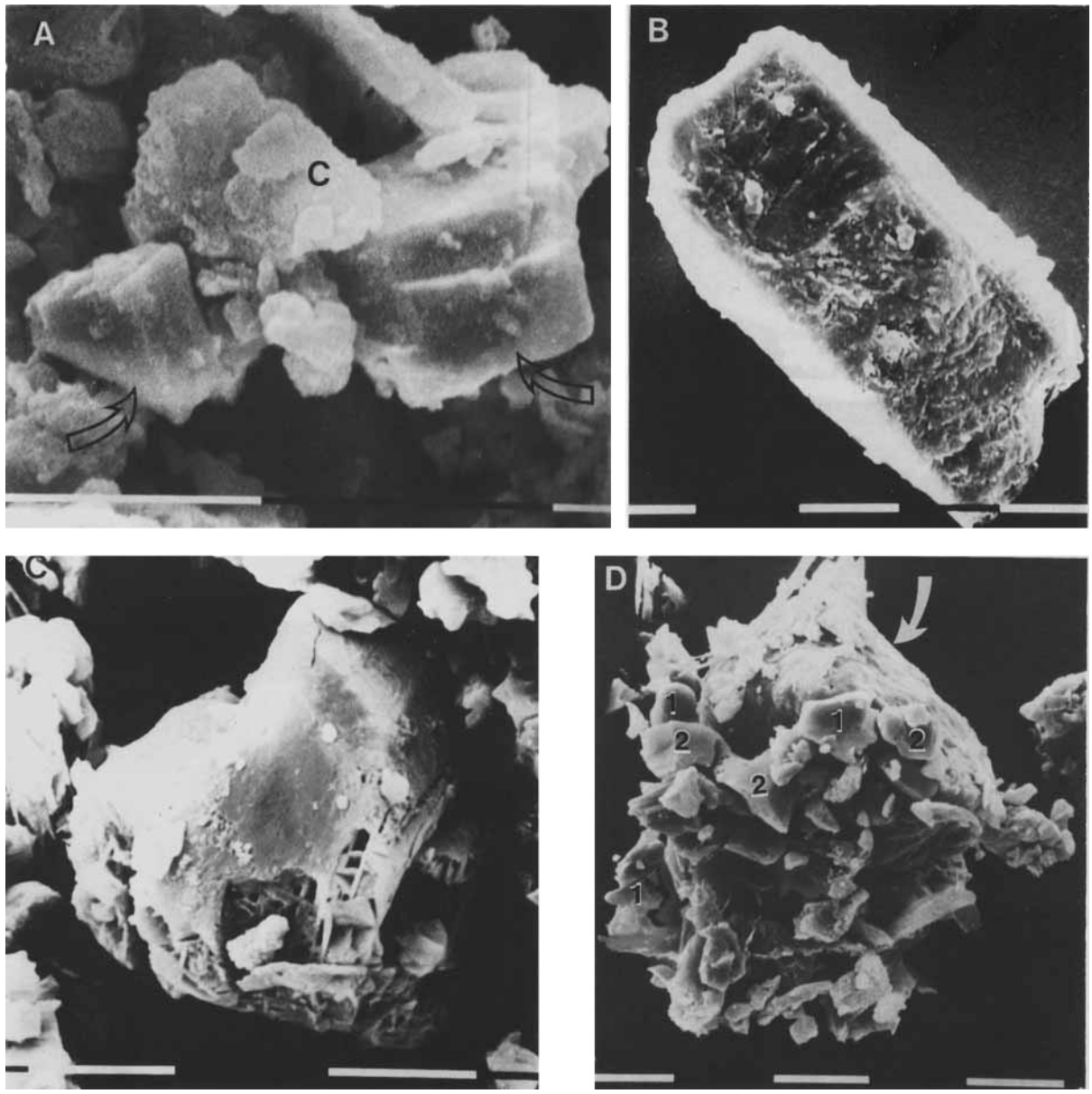

Figure 7. SEM views of spinel minerals. All scale-bars: 10 μm. (A) Detrital magnetite (arrows) and chromite (C) crystals (sample 5); (B) large, detrital chromite crystal (sample 4); (C) titanomagnetite fragment (sample 4); (D) spinel cluster of magnetite (arrow), chromite (1) and titanomagnetite (2) crystals (sample 4).

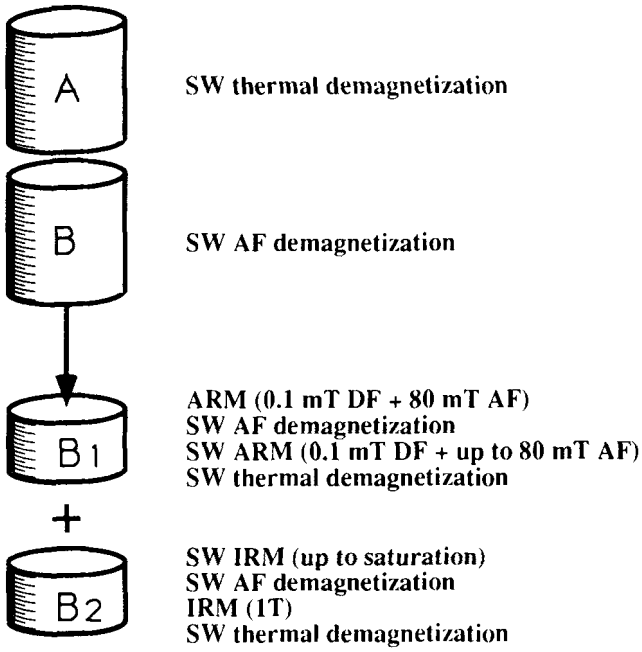

Figure 8. Outline of the treatments applied on fifteen 'test' samples in order to determine their magnetic mineralogy. SW: stepwise; ARM: anhysteretic remanent magnetization; IRM: isothermal remanent magnetization; DF: direct field; AF: alternating field.

temperature, leading to a steplike demagnetization curve (Dekkers 1989). Small grain pyrrhotite (smaller than 15 μm) has much higher coercivity than does magnetite (Dekkers 1988). Therefore, in order to characterize more precisely the complex mineralogy of our samples, we have first demagnetized the NRM of two samples at each level (Fig. 8), one thermally (A) and the other by AF (alternating field) treatment (B). The latter was cut into two pieces (B1 and B2). B1 was first remagnetized by ARM in a 0.1 mT continuous field superimposed on a 80 m T alternating field, and AF demagnetized in steps. Then it was remagnetized by ARM in steps up to 80 mT AF in a 0.1 mT continuous field, and finally stepwise thermally demagnetized. Subspecimen B2 was given a progressive IRM (until saturation was reached, in order to affect the high coercivity minerals), and stepwise AF demagnetized. Then it was remagnetized in a 1T field and finally thermally demagnetized in steps. The low-field susceptibility χ_0 of both subspecimens B1 and B2 was measured at each thermal step (up to 610 °C).

Results from sample 1, which is typical of the lowermost part of the section, are reported in Fig. 3. Thermal evolution of this sample clearly reveals the two-carrier mineralogy (Fig. 3b) and the increase of χ_0 after 350 °C (Fig. 3c). This increase is observed in all samples. Thermal cleaning of the NRM shows four successive components, the first two carried by pyrrhotite and, after 350 °C, two others carried by magnetite. The directions of the lower temperature component of these two groups are identical, and the very last component (560 to 580 °C) seems to have the same direction as the one ranging between 220 °C and 350 °C. We cannot distinguish between these four components in the AF treatment (Fig. 3d); the soft components carried both by the iron sulfide and the magnetite appear to be demagnetized at the same time.

In Fig. 3(b), we have plotted the evolutions of the intensities of NRM, ARM and IRM during heating, and each magnetization has been normalized to its maximum value. These three curves show two clear unblocking temperatures, a first one at ~320 °C, and a second one just before 600 °C. We see that the first two curves (NRM and ARM) are similar. Thus, the ratio of magnetization due to fine grained magnetite to that due to pyrrhotite is similar in NRM and ARM (75 per cent). IRM decreases faster than both NRM and ARM before 350 °C. Consequently, magnetic minerals with low unblocking temperatures seem to play a larger part in the IRM, acquired in a 1T field, than in the ARM, acquired under a 80 mT AF. These magnetic carriers of the IRM can be either multidomain (MD) magnetite, which is more affected by an IRM than by an ARM and becomes demagnetized at low temperatures (lower than 200 °C; McElhinny 1973), or high-coercivity pyrrhotite. The relative evolution of IRM and ARM upon heating is roughly similar in all 15 test samples.

The stepwise AF demagnetizatons of NRM, ARM and IRM are displayed in Fig. 3(e). Most of the IRM—which is more than six times larger than the ARM—disappears before a 40 mT AF cleaning, but one must be aware that a significant part of the IRM still remains at 90 mT. So this IRM must be mainly carried by large-grained MD magnetite, which easily loses its magnetization upon AF treatment (McElhinny 1973), but it is also carried by high coercivity pyrrhotite or ultra-fine magnetite (<0.01 μm; Collison 1983). These high-coercivity minerals must play an important part in the NRM, for the sample still retains 25 per cent of its initial magnetization after a 90 mT AF treatment.

We have performed a similar analysis of all 15 test samples defined above. These fall into distinct categories, which are used below to define six particular zones with given sets of magnetic properties. Sample 1 discussed above characterizes the lowermost zone. Five other samples, one for each zone, are now described.

The thermal demagnetization of the NRM, ARM and IRM from sample 5 (Fig. 9b), and also the AF demagnetizations (Fig. 9e) are distinctly different from those obtained for sample 1. The characteristic unblocking temperature of 320 °C is no more apparent in the ARM, and its AF demagnetization is easier than in sample 1. The ARM seems to be largely carried (up to 90 per cent) by magnetite. The ARM curves are similar for all upper (younger) zones (Fig. 10 to 13b and e), which implies a rather uniform grain size distribution of magnetite throughout the upper 600 m of the section. The thermal demagnetization of the NRM and IRM of sample 5 are essentially identical, and 80 per cent of these magnetizations disappear below 350 °C. The Curie point of pyrrhotite is more obvious on the NRM than IRM curve, while the NRM is slightly more resistant to AF demagnetization than the IRM. Therefore, IRM is carried by pyrrhotite and larger grain magnetite, while most of the NRM is carried by pyrrhotite. The contribution of pyrrhotite (80 per cent) can be deduced from the shape of the thermal demagnetization curve, for pyrrhotite loses its magnetization in a rather narrow range of temperature, and all removed magnetization outside of this range must be due to magnetite. The component of the NRM remaining beyond 350 °C,

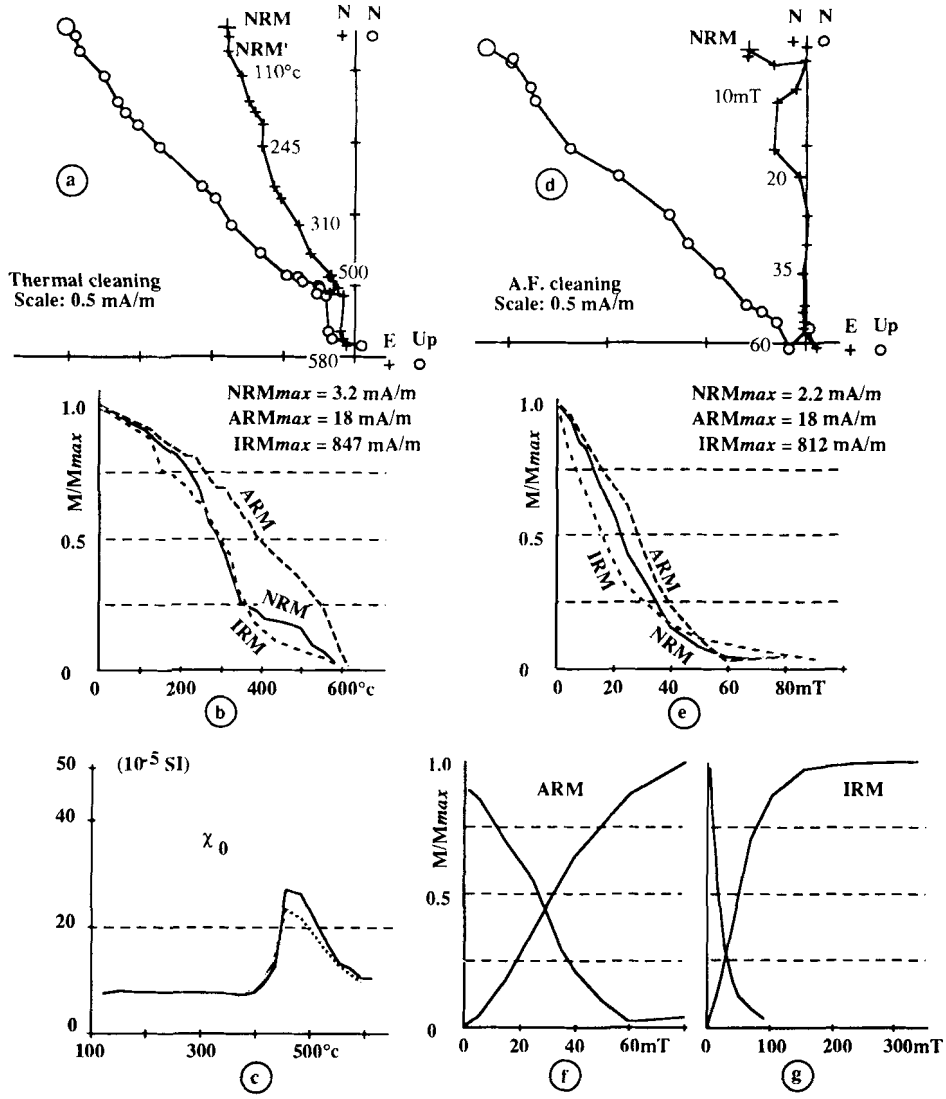

Figure 9. Same as Fig. 3, for sample 5.

amounting to 15 per cent of the total, is carried by magnetite and parallels the present earth field (PEF).

The thermal evolution of the NRM of sample 9 (Fig. 10a,b) is dominated by the fast removal of a PEF component below 220 °C. This component is also easily removed by AF, prior to 50 mT (Fig. 10d), and is apparently carried by larger grain magnetite. The underlying characteristic component is very noisy and can only be uncovered over few steps, between 220 °C and 300 °C; it amounts to some 20 per cent of the original NRM and is not removed by AF treatment up to 70 mT (Fig. 10d and e). This is likely carried by fine grain pyrrhotite (<15 μm; Dekkers 1988). Thermal demagnetization of the IRM does not reveal clearly the Curie point of pyrrhotite, which is likely to be hidden by the demagnetization of large grain magnetite. However, the same IRM has a larger coercivity than was the case for the two previous samples (compare Figs 10e, to 3e and 9e), which should mean that the part of the IRM carried by pyrrhotite lies within finer grains (<15 μm).

The same pyrrhotite appears to be the principal carrier of magnetization (NRM and IRM) in sample 10 (Fig. 11). Indeed, both thermal demagnetizations provide a clear pyrrhotite spectrum (Fig. 11b) and they are very resistant to AF treatment (Fig. 11e). The part of the NRM removed prior to 150 °C, and probably carried by large grains of magnetite, is parallel to the PEF. IRM is also partly carried by this magnetite as is seen from the thermal demagnetization curve below 200 °C and above 350 °C, for a total amount of approximately 25 per cent.

Despite the fact that it comes from a different zone, separated by the zone characterized by sample 10, sample 11 (Fig. 12) has essentially the same characteristics as sample 9 (Fig. 10). The thermal demagnetization of the NRM of sample 15 (Fig. 13) is somewhat reminiscent of that of sample 10. The fast fall of magnetization of sample 15 occurs at a slightly higher temperature (300 to 400 °C). However, AF demagnetization of this NRM is much easier, which may be due to large grain (>15 μm) pyrrhotite which has a smaller coercivity ($H_c \sim 50$ mT for a grain size of

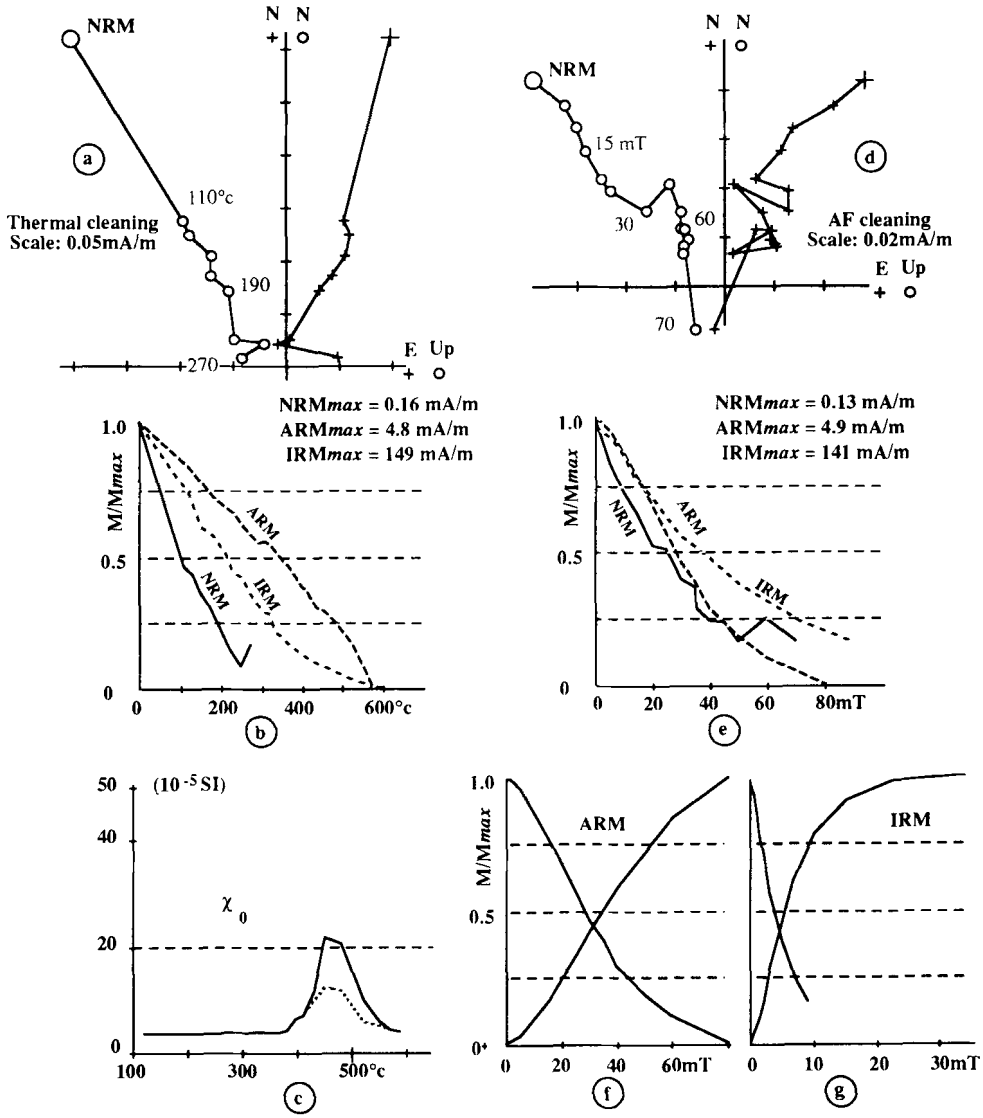

Figure 10. Same as Fig. 3, for sample 9.

15 μm). The behaviour of the IRM upon both AF and thermal cleaning is similar to that of samples 9 and 11 (Figs 10 and 12 respectively). This would imply the presence of both larger grain magnetite and pyrrhotite including finer grains which partly carry the IRM, with the NRM being carried by the larger pyrrhotite grains.

(e) Relative amounts of magnetic minerals

Through these experiments, we can also estimate the amounts of magnetite and of iron sufildes in each test sample. The importance of magnetite in the NRM varies significantly along the section, and we have tried to characterize the properties of this mineral in all 'test' samples. A phenomenological model has been developed by King *et al.* (1982) to help identify the relative grain size variations in the magnetite content of a sample, in which the χ_0 of each sample is compared to the ARM acquired after saturation, normalized by the constant field applied (in this case 0.1 mT). Use of this model is not straightforward in the case of the Stirone section, because of its complex mineralogy dominated by sulfides and magnetite (and not magnetite alone). However, the low-field susceptibility is mostly related to the magnetite fraction, because the χ_0 of pyrrhotite ($1–25.10^{-5}$ m^3 kg^{-1}) is an order of magnitude smaller than that of magnetite (Dekkers 1988). The ARM is certainly more sensitive to the sulfides, but most of the thermal demagnetization curves (except for the first three test samples from the lowermost part of the section) are characterized by a rather monotonic decrease up to 580 °C. It seems therefore that magnetite also plays a dominant role in this parameter. The other samples exhibit a change in the slope of the demagnetization curves above 350 °C. We can extrapolate the part of the curve above this step back to room temperature, keeping in mind that a significant portion of magnetite (mostly larger grains) was already demagnetized. We are thus dealing with the most resistant fraction mainly carried by small monodomain or pseudo-monodomain grains. On the other hand, the overall monotonic decrease of the demagnetization curves of the

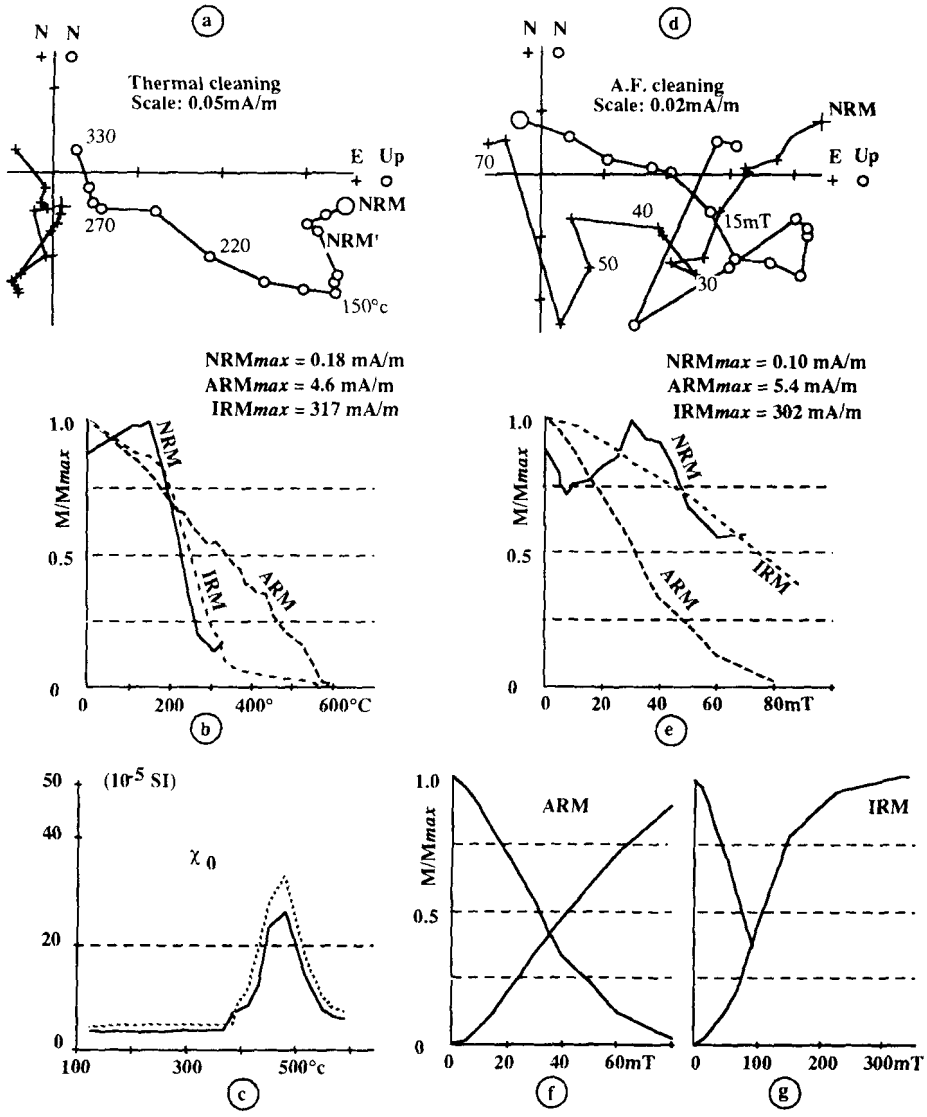

Figure 11. Same as Fig. 3, for sample 10.

ARM observed for the other samples, suggests that, at least to a first order, this approximation also reflects the original amount of total magnetite.

We have thus tentatively estimated the relative contribution of this mineral along the section by using the model of King *et al.* (1982). We are well aware that only relative changes in the amount of magnetite and relative grain sizes can be approached from the comparison of our data with the model. The values of χ_0 and ARM carried by magnetite are displayed in Fig. 14. The first three test samples from the lowermost part of the section contain single-domain (SD) magnetite (samples 1 and 2) or pseudo-single-domain (PSD) grains smaller than 1 μm (sample 3). In the rest of the section, magnetite grains appear to be larger and are either large PSD or multi-domain (MD). We can infer the percentage by weight of magnetite (relative to sample 3, arbitrarily taken to be 10) with this phenomenological model. This estimate of the relative amount of magnetite (RAM), plotted versus stratigraphic position on Fig. 15(a), decreases progressively from the bottom of the section up to the calcarenite 'C' (marking a major hiatus 400 m below the PPB), and remains constant above. With the exception of the lowermost part of section (samples 1 to 3), the large size of magnetite particles implies that they contribute little to the NRM of the samples after a thermal cleaning above 220 °C (less than 25 per cent). Indeed, no stable component can be observed in general above 350–380 °C in the NRM (e.g. Figs 10a to 12a). In the older samples, finer magnetite does carry a remanent component with the same direction as the sulfides (Fig. 3a) or, sometimes, in the direction of the present earth field (Fig. 9a).

Three parameters allow us to reckon the amounts of iron sulfides, and, more precisely, of ferromagnetic pyrrhotite. First, the increase of χ_0 after heating the sample up to 350 °C is due to the transformation of pyrite and both pyrrhotites into magnetite. This increase, normalized by the value of χ_0 before 350 °C ($\Delta\chi/\chi$), gives the ratio of the amount of newly formed magnetite to that of original magnetite. It then provides an estimate of the percentage of iron atoms held in sulfides in relation to those held in

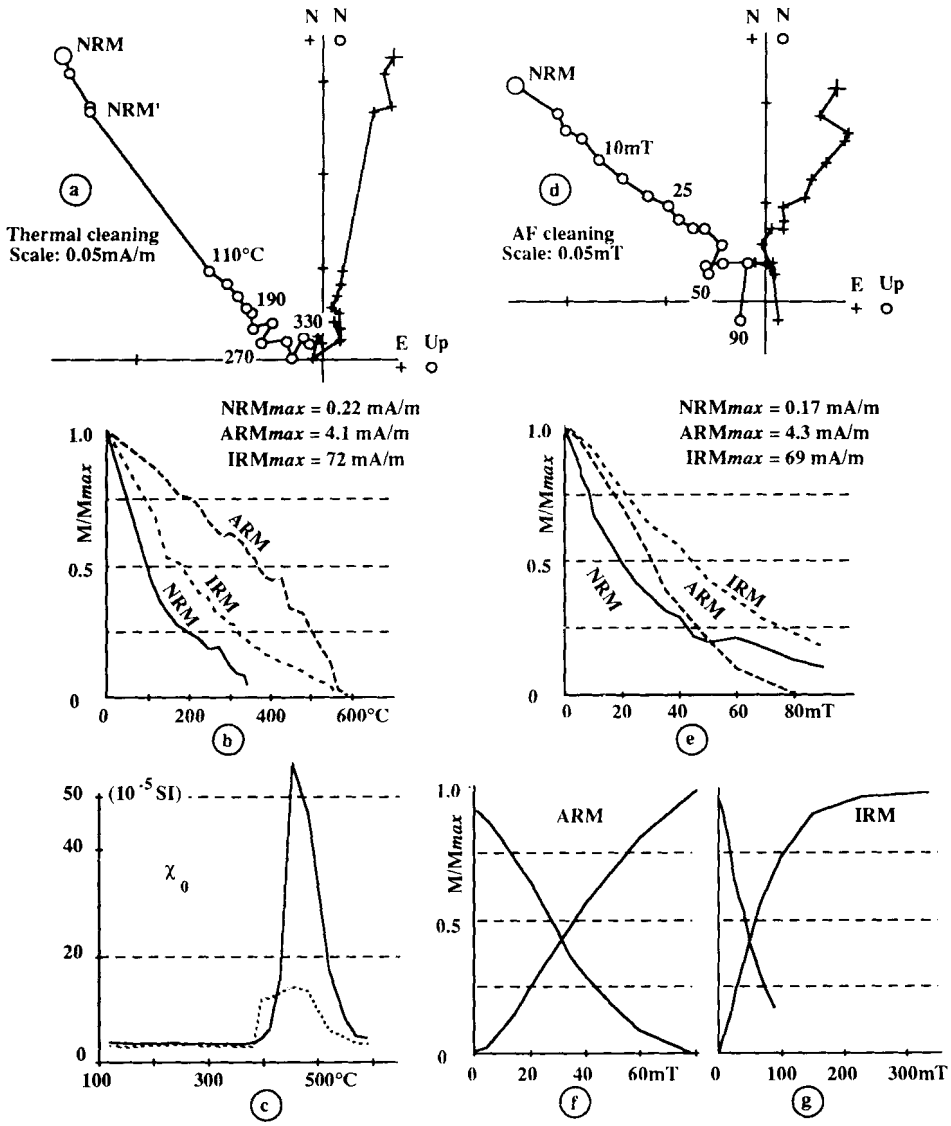

Figure 12. Same as Fig. 3, for sample 11.

magnetite (Fig. 15b). This ratio has been measured for two samples at each level. These two measurements are generally consistent, except for sample 11, just above the 'C' hiatus; at this level, there is no other anomaly in magnetic behaviour (Fig. 12), and the abnormal value of the $\Delta\chi/\chi$ ratio can be attributed to a larger amount of non-magnetic hexagonal pyrrhotite (Fe_9S_{10}) or pyrite. Otherwise, the relative importance of sulfides is found to increase with time, being on average larger in the upper half of the section than in the lower half (Fig. 15b).

In all cases when the thermal demagnetization of the IRM clearly features the superposition of magnetite and ferromagnetic pyrrhotite (i.e. below the calcarenite 'C', except at level 9—see Figs 3, 9 and 11), one can extrapolate the part of the curve above 350 °C (related to magnetite) back to room temperature. The difference between the total IRM at room temperature and this extrapolated IRM–M (for magnetite) reflects the contribution of the pyrrhotite, IRM–P. Both are shown in Fig. 15(a). A similar extrapolation applied on the ARM demagnetization curves shows that the ratio of the magnetization carried by low coercivity pyrrhotite (affected by an ARM) to that carried by magnetite is constant in samples 4 to 15. IRM–P, a proxy for the amount of pyrrhotite, and RAM (or IRM–M), a proxy for the amount of magnetite, evolve in parallel as a function of stratigraphic position (Fig. 15). It therefore seems that the total amounts of both magnetic pyrrhotite and magnetite decreased significantly with time in the lower half of the Stirone section. The increase in $\Delta\chi/\chi$ (and IRM–P/IRM–M) further indicates that as we move up, the relative contribution of iron sulfides increases.

Finally, the amount of high-coercivity pyrrhotite relative to that of lower coercivity magnetite can be approximated by the ratio of the IRM after AF cleaning up to 90 mT, to the IRM before any treatment (IRM_{90}/IRM_0). The maximum value of this parameter occurs beneath hiatus 'C' and corresponds to test sample 10 (Fig. 11). This is consistent with the sharp decrease of both NRM and IRM at

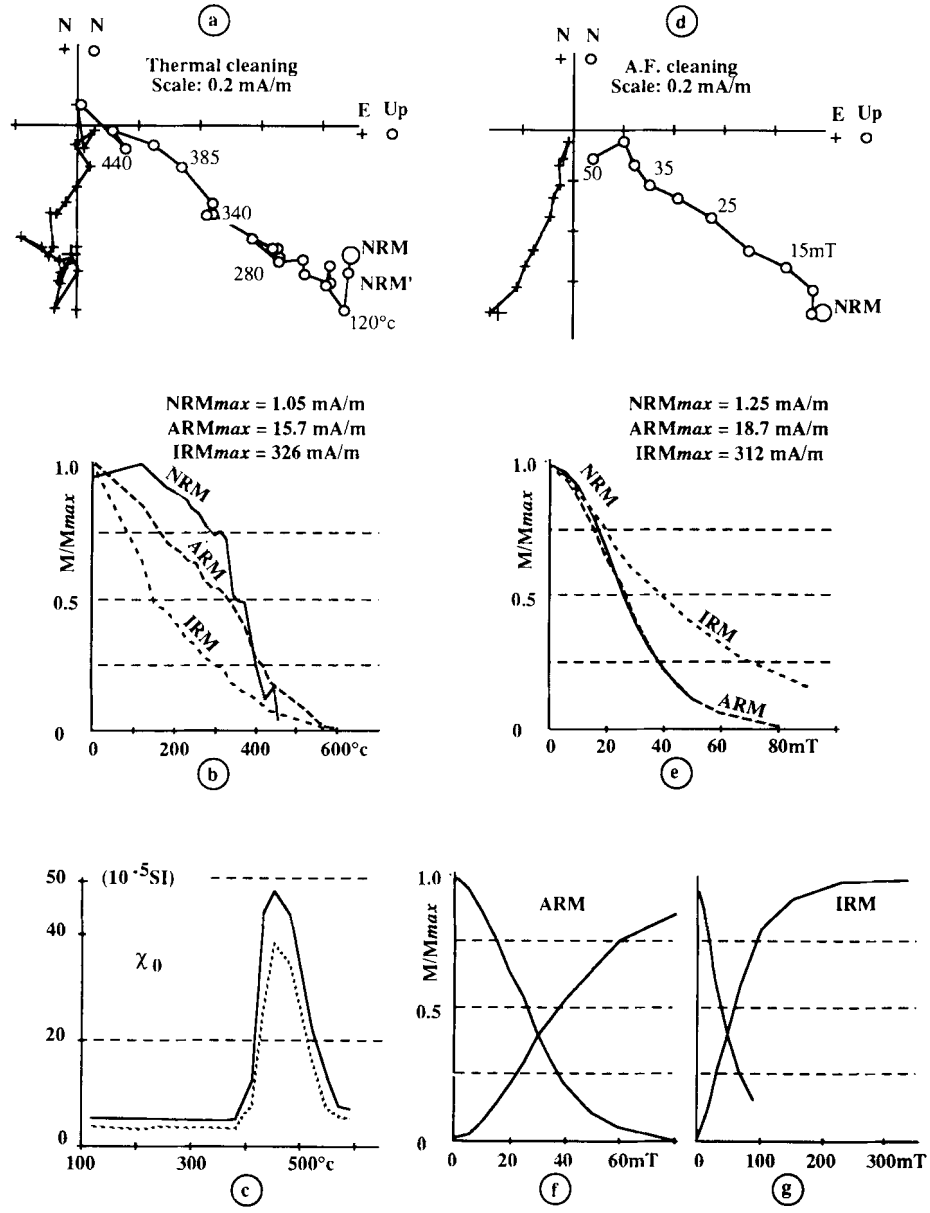

Figure 13. Same as Fig. 3, for sample 15.

150–270 °C during thermal demagnetization (Fig.11b), and their resistance to AF cleaning (Fig. 11e). It also corresponds to higher values of $\Delta\chi/\chi$. The saturation acquisition curve of this sample (Fig. 11g) gives an estimate of pyrrhotite grain size of 10–15 μm (Dekkers 1988). Below this sample, the ratio is nearly constant, which is consistent with the similarity of evolution of the amounts of iron sulfides (IRM–P) and magnetite (RAM). The relative contribution of ferromagnetic pyrrhotite is higher in the upper part of the section (samples 9 to 15), but this increase is not well correlated to the varation of $\Delta\chi/\chi$; the latter parameter corresponds to the whole iron sulfide fraction (i.e. pyrite, greigite and the two natural pyrrhotites), and the appearance of more Fe_7S_8 may correspond to the disappearance of other iron sulfildes (pyrite and non magnetic pyrrhotite).

(f) Magnetic carriers of the NRM along the Stirone section

Six zones have been defined, based on their magnetic properties. The six test samples described in detail above belong to each one of these zones. Fig. 16 gives stratigraphic logs of the median destructive temperature (MDT) and intensity of the NRM of all heated samples. Both logs correlate roughly. The zones therefore have reasonably uniform properties, and this is true for other available indicators. In zone I (test samples 1 to 3), the NRM is carried mainly (75 per cent) by fine grained (SD or PSD) magnetite and some (25 per cent) higher coercivity pyrrhotite, which accounts for both rather high MDT (of the order of 500 °C) and intensity. In zone II (test samples 4 to 8), the respective amounts of magnetite and pyrrhotite

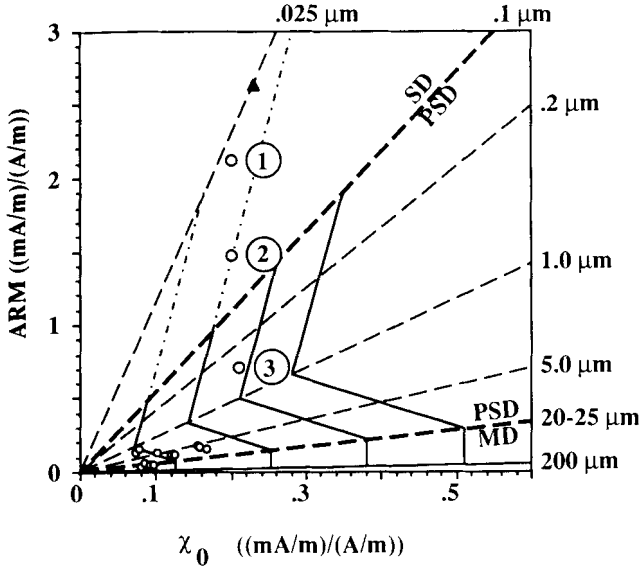

Figure 14. Plot of ARM (normalized to the constant field applied) versus initial susceptibility χ_0 for each 'test' sample (King *et al.* model, 1982). Samples '1' to '3' are labelled in circles. Dashed lines correspond to variations in the amount of magnetite of constant grain size (indicated at the end of the line). Broken solid lines correspond to constant amounts of magnetite of varying grain size. Triangle: sample with SD magnetite (0.025 μm), deduced from data given by King *et al.* (1982). Thicker dashed lines mark the boundaries between SD (single-domain) and PSD (pseudo-single-domain), and PSD and MD (multi-domain) magnetite.

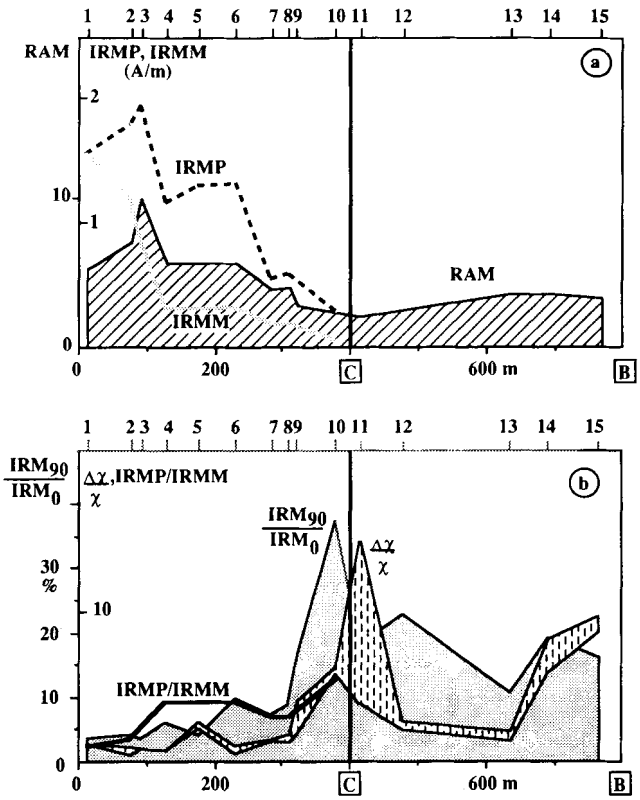

Figure 15. (a) Approximate values of relative quantities of magnetite and iron sulfides along the section; (a) RAM: relative amount of magnetite using the diagram (from King *et al.* 1982) in Fig. 5 (the third sample is arbitrarily taken to be 10); IRMP: part of the IRM (acquired at 1T) carried by the pyrrhotite; IRMM: part of the IRM (acquired at 1T) carried by the magnetite; (b) IRMP/IRMM: ratio of estimated pyrrhotite to magnetite contributions to the IRM; IRM_{90}/IRM_0: ratio of IRM before treatment to the remaining intensity after AF treatment of this IRM up to 90 mT; $\Delta\chi/\chi$: ratio of the increase of the initial susceptibility χ_0 after 400 °C to the value of χ_0 before 350 °C (determined on two samples at each level).

are reversed, hence the lower MDT (on the order of 300 °C) and intensity.

In zone III (test sample 9), the MDT is quite scattered and rather low. We attribute the lowest values (under 200 °C) to dominant (up to 80 per cent) MD magnetite. The large fluctuations in the MDT of the NRM are due to the vector superposition of the PEF component carried by this magnetite on top of a reversed polarity characteristic component carried by pyrrhotite. Zone V (test samples 11 and 12) has a very similar mineralogy, but the characteristic component tends to be normal, reducing significantly the scatter (with most MDTs below 200 °C).

The NRM from zones IV (test sample 10) and VI (test samples 13 to 15) is essentially carried by pyrrhotite (80 per cent), leading to MDTs similar to those in zone II (300 °C). Some of the samples in zone IV, just below the calcarenite 'C', are similar to surrounding samples from zones III and V, with a weaker MDT.

The main results of our mineralogical study are very roughly summarized in Table 1. The variations of amounts of the different magnetic minerals may be related to variations in sedimentation (relative amounts of organic matter and ferruginous supply, rate of sedimentation . . .). For example, zones IV and V are more sandy, and this might interfere in the succession of chemical reactions which lead to pyrite formation.

PALAEOMAGNETIC DIRECTIONS–MAGNETOSTRATIGRAPHY

The characteristic components were determined, for 90 per cent of the samples, by principal component analysis (Kirschvink 1980), with linear segments fit by least squares to at least 4 points (and often more) between 200 and 360 °C. Fisher means were used on samples which gave scattered demagnetization diagrams but which had an unambiguous polarity. All those directions are plotted in Fig. 17, with an indication of the range of directions obtained after correcting (dips vary from 25° to 40°) the direction of the PEF and its antipodal direction for bedding. Some samples (25) with discordant directions are indicated with smaller symbols. Some come from polarity transition zones. Others correspond to samples with an intensity much weaker than their neighbours. We have therefore retained only those sites for which several samples are internally consistent. We did not include these directions in the computation of the various means.

If we exclude samples with aberrant directions, we obtain two scattered antipodal clusters (Fig. 17). There is apparently no bias toward the direction parallel to the PEF, nor toward its antipodal direction. The reversed and normal average directions (RM and NM on Fig. 17, respectively) are antipodal at the 95 per cent confidence level. The overall

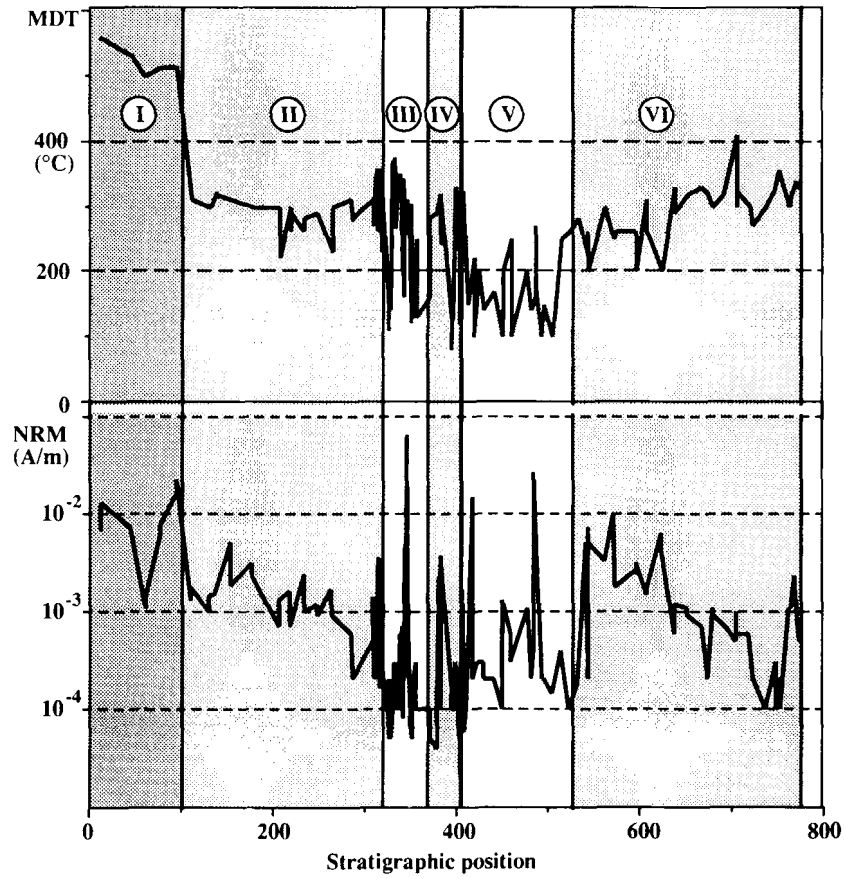

Figure 16. (a) Mean destructive temperature (MDT) of all heated samples, as a function of their stratigraphic position; I to VI: number of zones determined from the main characteristics of magnetic carriers. (b) NRM of all samples as a function of their stratigraphic position.

mean (GM) is at D = 0°, I = 52° (N = 199, K = 14, α = 3°). The declination is that expected for the present field (or recent field) at Parma and therefore demonstrates the lack of any signficant local rotation about a vertical axis. On the other hand, the inclination is some 11° (±3°) shallower than the expected one (63°). This cannot be attributed to a PEF overprint, since no significant bias of the NM and RM means is observed. Also the unblocking temperature spectra of the PEF overprint and characteristic component generally do not seem to overlap: the ranges are respectively NRM–360 °C and 500–580 °C for test sample 5 (Fig. 9a and b), NRM–150 °C and 150–300 °C for test sample 10 (Fig.

Table 1. Evolution of the main characteristics of magnetic minerals along the Stirone section, divided into six more or less uniform zones (labelled I to VI from bottom to top).

ZONES	I	II	III	IV	V	VI
Samples	1 2 3	4 5 6 7 8	9	10	11 12	13 14 15
Magnetite	SD-PSD	← PSD-MD →				
	Large RAM, decreasing (10 to 4)		RAM smaller, nearly constant (~4)			
(~% NRM)	75	25	75	25	75	25
Pyrrhotite	IRMS decreasing (/4)					
IRM_{30}/IRM_{0}	Slowly increasing		Increasing	Maximum	Large and erratic	
NRM carrier grain size	< 15μm	> 15μm	← < 15μm →			> 15μm
(~% NRM)	25	75	25	75	25	75

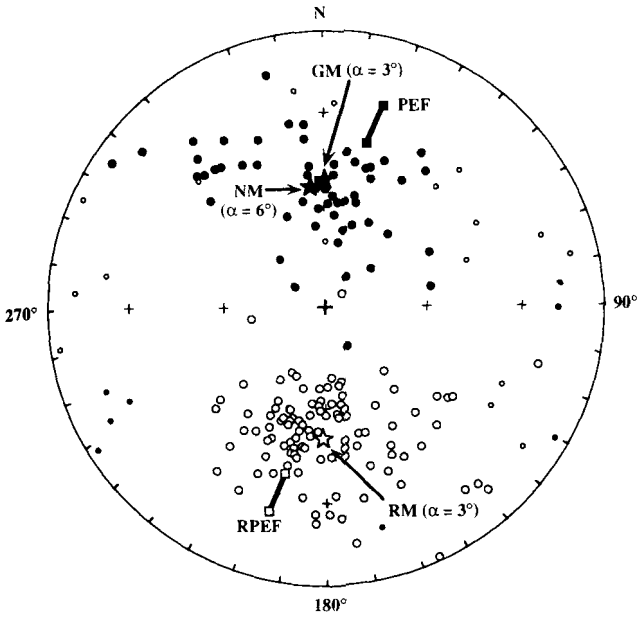

Figure 17. Lower hemisphere equal area projection of characteristic directions after tectonic correction. Open symbols: reversed directions; closed symbols: normal directions; small circles: aberrant directions, not considered in the the means. PEF: range of directions of the present earth's dipole field, after bedding corrections for all the dips of the section. RPEF: antipodal direction of the PEF, after the same bedding correction; GM: global mean; NM: normal mean; RM: reversed mean.

11a and b), NRM–210 °C and 210–350 °C for test sample 11 (Fig. 12a and b) and NRM –120 °C and 120–400 °C for test sample 15 (Fig. 13a and b). We therefore conclude that characteristic primary directions have undergone a ~10° inclination shallowing following deposition in these soft Pliocene clays. Such shallowing has been observed in sediments of similar lithology and have been the subject of recent work (Blow & Hamilton 1978; Morgan 1979; Laj *et al.* 1982). The mechanism for this shallowing is unclear in the case of the Stirone section. In particular, mechanical effects should not have had much effect on those sulfides which reside on or within calcitic spheres and foraminifera tests. It should have affected only the sulfides that were deposited within the bulk of the plastic clay matrix. Although the anisotropy of ARM or χ_0 can be used as indicators of inclination shallowing (Collombat, Rochette & Kent 1992), this method cannot be applied in the present case because both parameters are dominated by detrital magnetite, which is not the carrier of the characteristic NRM.

Individual characteristic components (D, I, and corresponding VGP latitude, which has not been corrected for inclination shallowing) are plotted in Fig. 18 (a, b and c respectively) according to their stratigraphic position. Over 95 per cent of the samples have a clearly normal or reversed polarity. The polarity sequence includes from bottom to top seven polarity zones (numbered A1 to A7) plus 10 m of aberrant directions with low inclination between 316 and 326 m (hatched in Fig. 18d) from the base up to the 'C' calcarenite and three zones (B1 to B3) from the 'C' calcarenite up to the 'B' calcarenite. The lowest *G. margaritae* occurs five meters below the first palaeomagnetic sample. The lowermost *Sphaeroidinellopsis seminulina* s.l. Zone has not been recorded (Iaccarino *et al.* 1992), and consequently, the base of *Globorotalia margaritae* Zone may also be missing. The base of the *Globorotalia margaritae–G. puncticulata* Zone occurs at 285 m (Fig. 2). The two zones are known to occur within the Gilbert polarity chron (Rio, Sprovieri & Raffi 1984; Glaçon, Rio & Sprovieri 1990; Rio, Raffi & Villa 1990; Rio, Sprovieri & Thunnell 1991). The Gilbert chron is interrupted by four normal subchrons (Thvera, Sidujfall, Nunivak and Cochiti from bottom to top). Because the FO of *G. margaritae* occurs within the normal Thvera subchron and our section begins with reversely magnetized rocks within the *G. margaritae Zone*, the Thvera subchron is suggested to be missing. The first samples must therefore correspond to the reversed interval immediately overlying the Thvera subchron. The FO of *G. puncticulata* falls within a reversed interval above the A4. Since in the Mediterranean and in particular in Italy, the FO of *G. puncticulata* occurs near the top of the Nunivak subchron at 4.15 Ma (Channell *et al* 1988)–4.13 Ma (Zijderveld *et al.* 1986), as is the case in the open Atlantic Ocean (e.g. Channell *et al.* 1990, Fig. 9), we correlate our two lowermost normal intervals (A2 and A4) with the Sidujfall and Nunivak subchrons, even if a very slight diachronism is suggested for the FO of *G. puncticulata* between the Stirone and other Italian sections. The ages quoted in this paper are from the Berggren (Berggren, Kent & van Couvering 1985; Rio *et al.* 1991) timescale unless specifically quoted otherwise. No direct data pertaining to dating are given in this paper so that any other scale, such as Harland *et al.* (1990) could have been used.

The interval of aberrant inclinations which occurs just above the base of *G. puncticulata–G. margaritae* Zone, is considered as a partly remagnetized zone (although one could argue that it hides a very thin normal interval) and the overlying normal interval A6 has been correlated with the Cochiti subchron.

The 'C' calcarenite separates sediments belonging to the *G. puncticulata–G. margaritae* Zone from those belonging to the *G. aemiliana* Zone. Therefore a hiatus involving the *G. puncticulata* Zone, the base of the *G. aemiliana* Zone, and probably the top of the *G. puncticulata–G. margaritae* Zone (corresponding to some 0.6–0.7 Ma) is involved. It follows that the top of the Gilbert reversed chron and the base of the Gauss normal chron are missing and the lower erosional surface of the 'C' calcarenite separates Zanclean from Piacenzian sediments.

Above the 'C' calcarenite, three main polarity zones have been recorded: a very short reversed one (B1), a normal one (B2) and a very long reversed one (B3). Between the latter two, a 30 m-thick transitional zone shown with hatches in Fig. 18(d) has been recorded. The biostratigraphic events characterizing the transitional zone and the B3 interval are the lowest occurrence of *B. marginata* at 500 m (thus dated at 5.5 Ma), and the LO of *G. bononiensis* at 613 m. The latter event, estimated at 2.4 Ma (Rio et al., 1991) and the FO of *G. inflata* at 1.99 Ma (Rio *et al.* 1991), fall below the PPB, within the Matuyama reversed chron, near the short Reunion normal subchrons (Raffi 1986). Because of the co-occurrence of *G. aemiliana* and *G. bononiensis* and the length of chron B3, B1 and B2 are considered to correspond

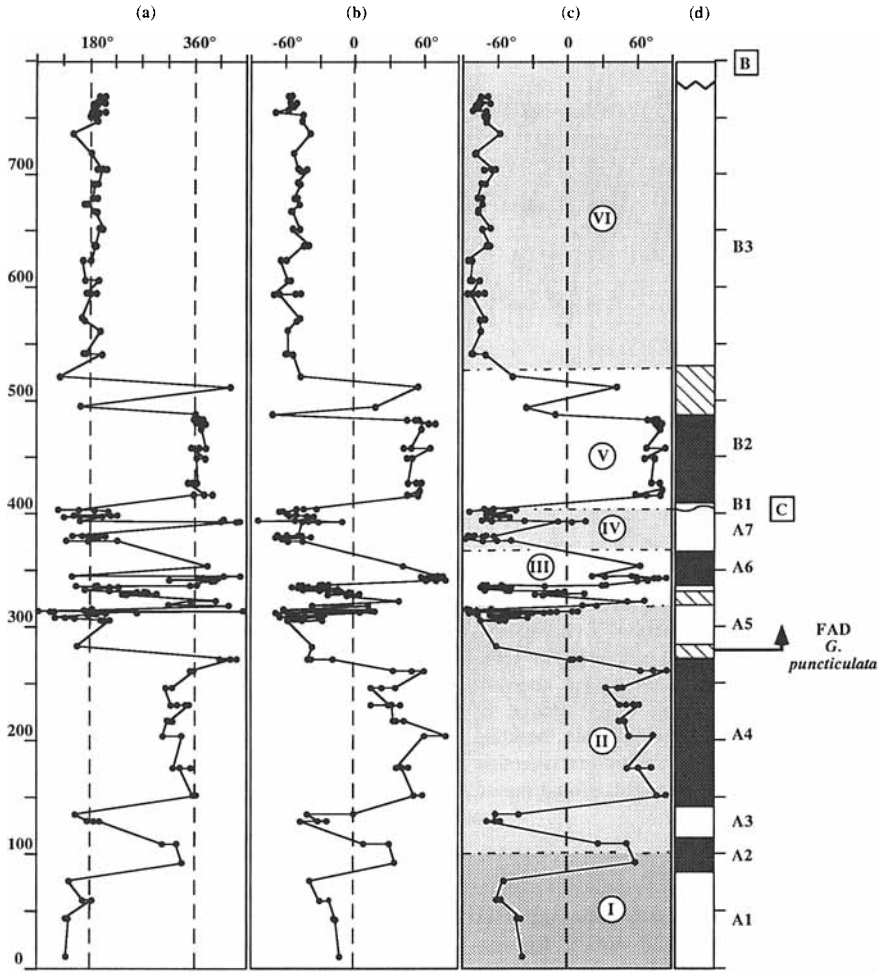

Figure 18. (a) Declination and (b) inclination of characteristic magnetic directions; (c) variations of VGP latitude. Mineralogical zones I to VI are from Fig. 16; (d) proposed magnetostratigraphy for the Stirone section and biostratigraphic events. Polarity zones are numbered from A1 to A7, and B1 to B3.

to the Kaena reversed subchron and the end of the Gauss normal chron respectively, and B3 to the lower part of the Matuyama reversed chron. The complex transitional interval must therefore be the Gauss/Matuyama transition. Evidence of short normal events within the B3 chron have not been detected, despite a high sedimentation rate (> 200 m/Ma) and rather dense sampling (Fig. 18). Therefore, it is suggested that the Reunion and Olduvai subchrons are missing, despite the fact that the last analysed samples have been collected about 30 m below the PPB. The absence of *G. inflata* within this interval supports this suggestion.

Unpublished palaeomagnetic data are available for the upper part of the Stirone sequence including also the lowermost Pleistocene (Bucha *et al.* 1975; Besse & Kukla 1985, personal communication), and are shown in Fig. 2(b). In this upper part of the sequence, the strata are quite flat-lying, so that unrecognized remagnetization in the present geomagnetic field could be interpreted as normal polarity zones. According to Bucha *et al.* (1975) normal polarity zones are recorded only in the Pleistocene interval. Unfortunately, the stratigraphic positions of the Bucha data are approximate; in fact no detailed indications were published and only a personal communication to the University of Parma could be found in Raffi (1982). The uppermost part (the last 80 m) of the Pliocene section has also been studied by Besse & Kukla (1985, personal communication; see Figs 2b and 19i). They tentatively suggested that the sandy levels between 55 m and 75 m below the PPB could normally be magnetized, but our study shows that they must have suffered remagnetization in the PEF. The PPB based on the FO of *A. islandica*, occurs just above a thick calcarenite bed ('B' on Fig. 19i) in a reversed zone. *H. baltica* appears above, still in a reversed interval, a few meters below a normal interval which is unfortunately interrupted by a gap in sedimentation. There are apparently significant fluctuations in sedimentation rate and two more unconformities are recognized within reversely magnetized clays and sandy clays. Finally, the last samples provide evidence for a normal interval which can only be attributed to the Brunhes chron. Therefore according to the Besse and Kukla data, the section falls essentially within the Matuyama chron and the normal polarity interval above the FO of *H. baltica* is correlated with the Jaramillo subchron.

COMPARISON WITH OTHER SECTIONS

We correlated the biomagnetostratigraphic results from this paper, with those of other sections from the Mediterranean

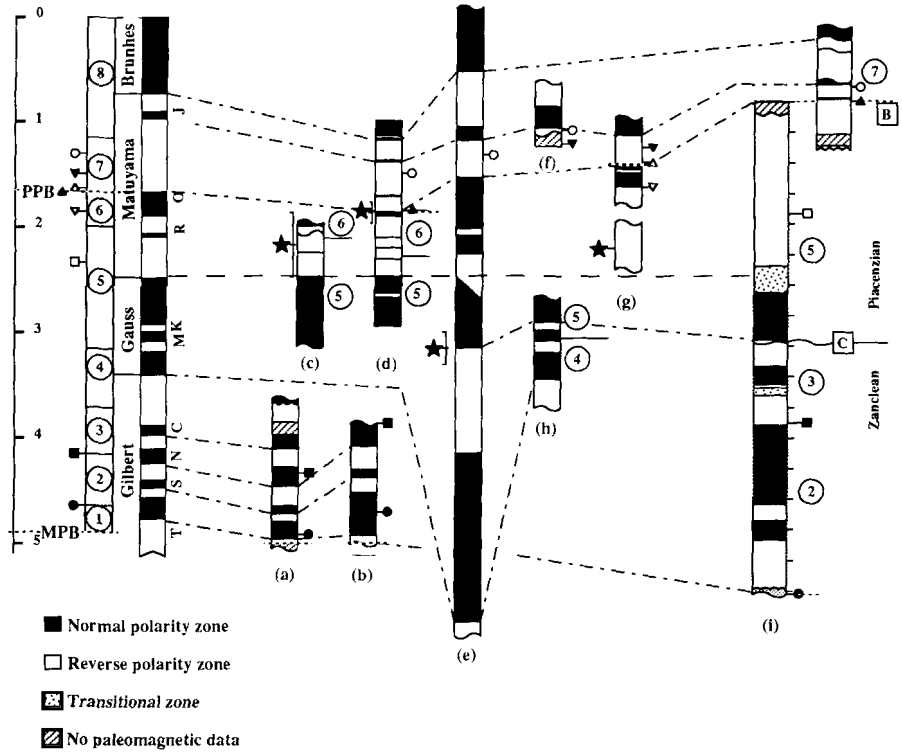

Figure 19. Correlation between magnetostratigraphic columns obtained in Mediterranean sediments and the geomagnetic reversal time scale (Berggren *et al.* 1985). (a) Singa & Roccella sections (Zijderveld *et al.* 1986), (b) Capo Spartivento section (Channell *et al.* 1988), (c) Valle Ricca quarry (Arias *et al.* 1980, 1990), (d) Santerno section (Nakagawa 1977), (e) Rhodos Island (Lovlie *et al.* 1989), (f) Croce Valanidi section (Aïfa *et al.* 1988), (g) Vrica section (Tauxe *et al.* 1983), (h) Capo Roccello section (Zachariasse *et al.* 1989), (i) Stirone section, this study (see Figs 2 and 18). Sections are aligned at the Gauss–Matuyama polarity transition (dashed line), when observed. Star: absolute ages measured, aligned with the correct value on the age axis. Numbers in circles: biostratigraphic zones; (1) *Sphaeroidinellopsis seminulina* Zone; (2) *G. margaritae margaritae* Zone; (3) *G. margaritae–G. puncticulata* Zone; (4) *S. subdehiscens* Zone; (5) *G. aemiliana* Zone (=*G. Gr. crassaformis* Zone); (6) *G. inflata* Zone; (7) *G. cariacoensis* Zone; (8) *G. truncatulinoides excelsa* Zone. Open circle: FAD *H. baltica*; black triangle, pointing down: LAD *C. macintyrei*; open triangle, pointing up: FAD *C. testudo*; black triangle, pointing up: FAD *A. islandica*; open triangle, pointing down: LAD *D. brouweri*; open square: LAD *G. bononeniensis*; black square: FAD *G. puncticulata*; Black circle: FAD *G. margaritae*; MPB: Mio–Pliocene boundary; PPB: Plio–Pleistocene boundary.

area (Fig. 19). Besides the Stirone section, eight other sections, available in the literature, have been considered.

In Fig. 19, all sections have been aligned arbitrarily at the Gauss–Matuyama reversal boundary (when found). When available, absolute (radiometric) ages have been indicated by a star. These have been aligned with the correct value on the age axis at the left of the figure. Reference is made again to the time scale and biochronology reported in Rio *et al.* (1991) and to the zonal scheme of Iaccarino (1985). Pliocene and Pleistocene biozones from the *Sphaeroidinellopsis seminulina* s.l. Zone to the *Globorotalia truncatulinoides excelsa* Zone are numbered from 1 to 8; the most significant bioevents are indicated with different symbols.

The first two sections come from Calabria (Zijderveld *et al.* 1986; Channell *et al.* 1988; Fig. 19a and b). They both show the Mio/Pliocene boundary in a reversed interval, below the Thvera subchron and the FO of *G. margaritae* and *G. puncticulata* within the Thvera and Nunivak subchrons respectively. Consistent ages are found for these three events (Hilgen & Langereis 1988; Zijderveld *et al.* 1986; Channell *et al.* 1988; Channell *et al.* 1990); these authors used the Berggren *et al.* (1985) time scale, and estimated an age of 4.8 to 4.9 Ma for the MPB, and 4.6 Ma and 4.1 Ma respectively for the two FOs. Rio *et al.* (1991) reported the same ages for these events.

Fig. 19(c) displays a sequence from central Italy, North of Roma (Arias *et al.* 1980, 1990); it consists of a composite section (the Tini and Silpa pits) and a drill hole (175 bis) located in the same quarry in the Valle Ricca. We resampled an interval around the ash layer (dated by fission tracks at 2.1 ± 0.2 Ma) which was originally thought to have normal magnetization (Arias *et al.* 1980), and found it to have been insufficiently demagnetized. In fact, heating to 280 °C revealed a clear reversed primary component which has been reported in Fig. 19(c). It is suggested that the *G. inflata* Zone is present on the base of palaeomagnetic data and radiometric age of the ash layer (Arias *et al.* 1990). The composite section yields an extrapolated age of 2.0 Ma for the boundary between the *G. aemiliana* Zone and the *G. inflata* Zone.

The Santerno section (Nakagawa 1977; and Fig. 19d) has been extensively criticized by Kukla (Kukla, Collins & Bender 1979). Therefore the estimated ages originally taken as reference cannot be used anymore. They were 2.3 Ma for the *G. aemiliana–G. inflata* Zone boundary, 1.6 Ma for the PPB and 1.2 Ma for the FO of *H. baltica*.

Fig. 19(e) results from a synthesis of three nearby sections in the Rhodos island (Lovlie *et al.* 1989). The identification of the FO of *H. baltica* recorded below a normal polarity interval is the only event recognized in the composite section. If correct, the interpretation by the authors reproduced in Fig. 19(e) implies an age of 1.3 Ma for the FO of *H. baltica*, placed between the Olduvai and Jaramillo normal subchrons.

Fig. 19(f) shows the magnetostratigraphy from Croce Valadini section in Calabria (Aïfa *et al.* 1988). The FO of *H. baltica* occurs just below a normal zone interpreted as Jaramillo, with an age of 1.0 Ma.

In Sicily (Punta Grande and Punta Piccola sections), Zachariasse *et al.* 1989 (Fig. 19h) recorded the Gilbert–Gauss boundary and the *S. subdehiscens–G. elongatus* Zone boundary which falls between the Kaena and Mammoth subchrons, at 3.1 Ma.

The Vrica section (Fig. 19g) is a composite of two distinct parts. The lower part is entirely reversed and contains an ash layer dated at 2.2 Ma. The PPB falls in the upper part just above two normal zones (Tauxe *et al.* 1983) identified with the single Olduvai subchron. The reversed layer in between is interpreted as a complex transition, similar to that observed elsewhere (Tric *et al.* 1991; Herrero-Bervera & Theyer 1986). Moreover, they interpret the topmost normal zone as an event between Jaramillo and Olduvai. If correct, this interpretation would invalidate that of the Croce Valadini section (Fig. 19f) and the inferred *H. baltica* age, but we doubt it and do interpret the top of the Vrica section as being Jaramillo (because of the correlative LO of *Calcidiscus macintyrei*).

Let us now summarize the information provided by the Stirone section in this general framework. The MPB begins within a reversed interval above the Thvera subchron (compare Fig. 19a, b and i). The FO of *G. puncticulata* occurs just above the Nunivak subchron whereas it occurs within the Nunivak in the Calabrian and Sicilian sections. This would imply some diachronism between Southern Italy

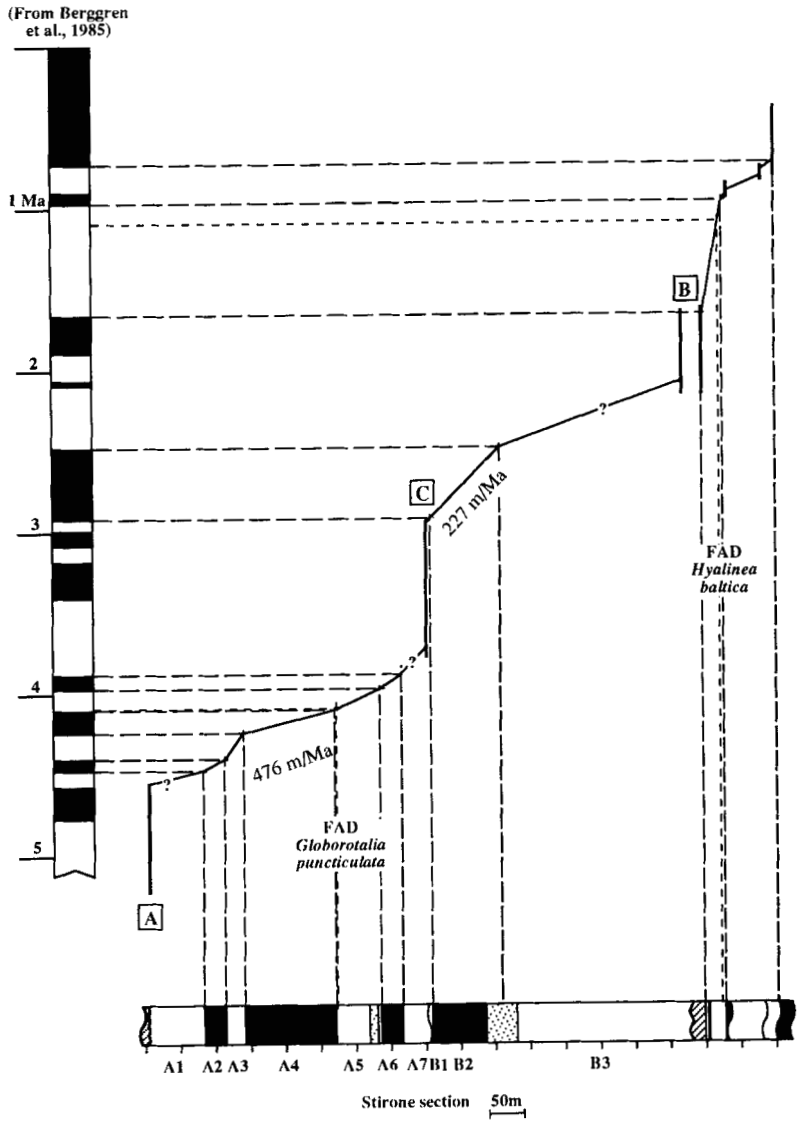

Figure 20. Correlation of the magnetostratigraphy obtained in the Stirone section (Figs 18 and 19) with the magnetic reversal time scale (Berggren *et al.* 1985).

where it first appears at 4.15 Ma (Channell *et al.* 1988) and the Po Valley where the species appears a little later (at about 4.1 Ma).

The Gauss–Matuyama reversal boundary is rather safely identified in the upper part of the Stirone section, and is very useful because it constrains the age of the LO of *D. pentaradiatus*: this event is observed 540 m above the MPB, and its extrapolated age is 2.4 Ma, which is its estimated age (Rio *et al.* 1990). This upper part of our section (above the 'C' calcarenite) begins earlier than the sections at Valle Ricca and Santerno (Fig. 19c and d) within the top of the Kaena reversed subchron, also seen at Capo Rossello (Fig. 19h) and Rhodos (Fig. 19e), where an age of 3.1 ± 0.1 Ma is determined. Our section therefore provides an upper bound (because the actual base of the zone is missing) for the beginning of the *G. aemiliana* zone at 2.9 Ma.

Finally, the FO of *H. baltica* within the overlying Pleistocene sequence just below the beginning of what is interpreted as being the Jaramillo subchron leads to an estimated age of 1.1 Ma for this event based on the sedimentation rate which is consistent with that estimated at Santerno, Rhodos and Croce Valadini (Fig. 19d, e and f). Our interpretation of the Stirone section is displayed in Fig. 20 against the time scale reported in Rio *et al.* (1991) showing the evidence for three major gaps in sedimentation and leading to average sedimentation rates of 470 m Ma^{-1} in the lower half, 200 m Ma^{-1} in the central part and more than 400 m Ma^{-1} in the uppermost part. The rate is, however, rather irregular, the gaps lasting about 0.6–0.7 Ma below the 'C' calcarenite and between 0.4 and 0.7 Ma below the 'B' calcarenite.

CONCLUSION

Much of the Pliocene crops out along a 4 km exposure of dominantly blue clays along the Stirone River near Parma (Italy), although the presence of some sandy levels and two distinct calcarenite beds, respectively 20 m and 395 m below the PPB, clearly indicate changes in the sedimentation processes and possible gaps. Hiatuses were even more frequent above the PPB at 34, 85 and 100 m. Biostratigraphic analyses made it possible to locate precisely the FO of *G. puncticulata, A. islandica* and *H. baltica*. Much of the early Piacenzian was found to be missing.

Previous magnetostratigraphic analyses of Mediterranean Plio–Pleistocene sediments had revealed a complex magnetic mineralogy with in general at least two distinct magnetic carriers. At the Stirone section, we singled out 15 levels for more detailed analysis. Thermal demagnetization of the NRM in general revealed two ranges of unblocking temperatures, at 100–300 °C and 450–600 °C, consistent with co-existing sulfides and magnetite. Curie balance thermomagnetic analysis confirmed the presence of magnetite with an iron sulfide, with up to 75 per cent of the saturation remanence of the unheated specimen residing in the latter. X-ray diffraction yielded magnetite spectra, and pyrite and pyrrhotite were sometimes recognized. Coupled SEM-microprobe analysis provided evidence for large grains of detrital magnetite, some titanomagnetite and chromite, pyrite and non-magnetite pyrrhotite and, possibly in one instance, greigite. Maghemite could in all instances be excluded, and greigite, if present, is a minor element contrary to the nearby Crostolo section (Tric *et al.* 1991). The iron sulfides, which were so obvious in the thermal experiments, did not show up conclusively in the other analyses. However, both tiny magnetite and iron sulfide crystals were observed pasted on calcitic spheres which could be identified as transformed foraminifera and iron sulfides were once observed within a foraminifera. There is therefore interesting evidence of a genetic link between the two and this may be responsible for the difficulty in magnetically extracting the sulfides from the sediments. This also suggests development of these sulfides early in the sedimentation process.

Samples were given an ARM and an IRM and the demagnetization of the two (plus the NRM) were compared upon thermal and AF cleaning. Low-field susceptibility χ_0 was measured in order to monitor mineralogical changes; indeed an increase of χ_0 beyond 350–400 °C was always observed, indicative of the transformation of iron sulfides. Differences in behaviour of the three magnetizations upon demagnetization were interpreted in terms of PSD or MD magnetite and generally dominant high-coercivity pyrrhotite in varying amounts and grain sizes. The relative contribution and grain sizes of magnetite were estimated using a χ_0–ARM diagram following the model of King *et al.* (1982). In cases when thermal demagnetization of the IRM clearly revealed the presence of both minerals, we extrapolated the part of the curve above 350 °C (related to magnetite alone) back to room temperature and used this to estimate the relative contributions to these minerals. We found the importance of both magnetite and pyrrhotite to decrease upsection, with the relative contribution of the latter increasing. Another useful parameter was the increase in χ_0 above 350 °C which provided an estimate of iron atoms held in sulfides with respect to those in magnetite. Finally, the ratio of IRM after AF cleaning to 90 mT to that before treatment images the relative amounts of high-coercivity pyrrhotite relative to lower coercivity magnetite. Both last indices roughly increased upsection, with a peak, or irregular fluctuations near the calcarenite bed marking the condensed or missing middle Pliocene near the middle of the section. Taken altogether, these five rough magnetic indicators gave a consistent picture of decreasing importance of magnetite and increasing influence of pyrrhotite in various grain sizes, allowing us to divide the section into six more or less uniform zones labeled I to VI from bottom to top.

Except in zone I where magnetite was also a carrier, pyrrhotite in the 150–350 °C range was taken to be the main carrier of the characteristic (hopefully quasi-primary) magnetization. About 10 per cent of the samples display transitional or weak and erratic directions. The rest form two scattered but antipodal (at the 95 per cent confidence level) clusters with no indication of a PEF bias. The overall mean in stratigraphic coordinates (dips vary from 40° to 25° in a NNE direction) is $D = 0°$, $I = 52°$ ($N = 199$, $K = 14$, $\alpha_{95} = 3°$). Inclination is some 10° shallower than expected, which we interpret this to be due to synsedimentary inclination shallowing (with an unclear mechanism).

Magnetostratigraphy displays a sequence of 10 polarity zones (A1 to A7 below the 'C' calcarenite bed and B1 to B3 above up to the PPB). Biostratigraphic markers allow some unambiguous correlations with the reversal time scale.

The Stirone section begins with a reversed zone, just above the Thvera subchron (within the Gilbert chron). The Sidujfall, Nunivak and Cochiti subchrons are identified. The first part of the early Pliocene ends with the calcarenite bed 'C' in a reversed zone, near the top of the Gilbert chron. The FO of *G. puncticulata* occurs at the bottom of a reversed zone which we interpret to fall between the Nunivak and Cochiti subchrons. If correct, our interpretation would imply a diachronous age of the FO of *G. puncticulata,* which first appears within the Nunivak subchron elsewhere (Zijderveld *et al.* 1986; Channell *et al.* 1988) (Fig. 19). The sedimentation rate for the Zanclean interval (398 m thick, shorter than 1.1 Ma) is about 470 m Ma^{-1}, although it is clearly not uniform. The 'C' calcarenite indicates a sedimentation gap of 0.6 Ma. The thin reversed, thick normal and even thicker reversed zones above 'C' are correlated to the top of Gauss and much of Matuyama. The Gauss–Mutuyama reversal boundary is a thick and complex zone, probably partly due to complex remagnetization, partly to an actually complex transitional record. This may also (unfortunately) be related to a mineralogical transition (boundary between zones V and VI). This second phase of sedimentation is about 375 m thick and 1 Ma long, corresponding to a sedimentation rate of about 300 m Ma^{-1}. The 'B' calcarenite indicates a sedimentation gap of at least 0.4 Ma. When sedimentation resumes in the Pleistocene, it is apparently even less uniform, with at least three gaps encountered in the magnetostratigraphy by Besse & Kukla (1985, personal communication; and Figs 2 and 19). Two narrow normal zones are found within a dominantly reversed interval, bounded by an unconformity in their lower and upper parts respectively. The simplest interpretation is that the lower one corresponds to Jaramillo and the upper one to the Brunhes–Mutuyama boundary. Because of unconformities, the Olduvai and Reunion subchrons remain unobserved.

A comparison of some available magnetostratigraphic Plio–Pleistocene sections from the Mediterranean area (Fig. 19) with the Stirone section suggests that the Stirone section, despite its many sedimentary and mineralogical complexities, yields a number of interesting constraints; the three more important ones appear to be the age of the FO of *G. puncticulata* (appearing at the same level as the top of the Nunivak subchron) at 4.1 Ma, the lowest occurrence of *B. marginata* immediately above the Gauss–Matuyama boundary and the age of the FO of *H. baltica* at 1.0 Ma, in agreement with (although possibly slightly younger than) previous estimates at three sections (Fig. 19, Nakagawa 1977; Aïfa *et al.* 1988; Lovlie *et al.* 1989).

ACKNOWLEDGMENTS

We thank G. Kukla, Y. Chen, Y. Gallet, J. P. Valet and R. Weeks for help in the field, G. Kukla for allowing us to use unpublished data, B. Clozel for help with the X-ray observations, E. Tric and P. Rochette for comments and making a preprint available, and J.P. Valet for reading a preprint of the paper and making valuable comments and suggestions. Finally, we are grateful to particularly careful reading by an anonymous referee. All correspondence should be sent to V. Courtillot. IPG contribution NS 1179.

REFERENCES

Aguirre, J. & Pasini, G., 1985. The Pliocene–Pleistoene boundary, *Episodes,* **8,** 116–120.

Aïfa, T., Feinberg, H. & Pozzi, J. P., 1988. Pliocene–Pleistocene evolution of the Tyrrhenian arc: paleomagnetic determination of uplift and rotational deformation, *Earth planet. Sci. Lett.,* **87,** 438–452.

Arias, C., Azzaroli, A., Bigazzi, G. & Bonadonna, F., 1980. Magnetostratigraphy and Pliocene–Pleistocene boundary in Italy, *Quarternary Res.* **13,** 65–74.

Arias, C., Bigazzi, G., Bonadonna, F. P., Iaccarino, S., Urban, B., Dal Molin, M., Dal Monte, L. & Martolini, M., 1990. Valle Ricca Late Neogene sytratigraphy. *Paleobiolog. continentale,* Montpellier, **17,** 61–80.

Backman, J., Shackleton, N. J. & Tauxe, L., 1983. Quantitative nannofossil correlation to open ocean deep-sea sections from Plio–Pleistocene boundary at Vrica, Italy, *Nature,* **304,** 156–158.

Barbieri, F., 1967. The foraminifera in the Pliocene section Vernasca–Castell'Arquato including the 'Piacenzian stratotype' (Piacenza province), *Mem. Soc. Ital. Sci. Nat.,* Milano, **15,** 145–163.

Bassett, M. G., 1985. Towards a 'Common Language' in stratigraphy, *Episodes,* **8**(2), 116–120.

Berggren, W. A., Kent, D. V. & Van Couvering, J. A., 1985. The Neogene: Part 2, The Neogene geochronology and chronostratigraphy, in *Geol. Soc. London Mem.,* **10,** 251–260.

Berner, R. A., 1983. Sedimentary pyrite formation: an update, *Geochim. Cosmochim. Acta,* **48,** 605–615.

Bertolani Marchetti, D., Accorsi, C. A., Pelosio, G. & Raffi, S., 1979. Palynology and stratigraphy of the Plio–Pleistocene sequence of the Stirone River (Northern Italy), *Pollen et Spores,* **21,** 150–167.

Blow, R. A. & Hamilton, N., 1978. Effect of compaction on the acquisition of a detrital remanent magnetization in fine-grained sediments, *Geophys. J. R. astr. Soc.,* **52,** 13–23.

Bucha, V., Horacek, J., Koci, A., Sibrava, V. & Lozek, V., 1975. Paleomagnetic correlations of Pleistocene sediments of Central Europe, *Quaternary Glaciations in the Northern Hemisphere,* **2,** 9–36.

Capotondi, L., Iaccarino, S., Mary, C., Pugliese, N., Vergnaud Grazzini, C., Butturini, F., Mora, S., Paperi, A. & Turco, E. 1990. *The Pliocene sequence of the Stirone River,* (in press) Parma, Italy.

Channell, J. E. T. & Hawthorne, T., 1990. Progressive dissolution of titanomagnetites at ODP Site 653 (Tyrrhenian sea), *Earth planet. Sci. Lett.,* **96,** 469–480.

Channell, J. E. T., Rio, D., Sprovieri, R. & Glaçon, G., 1990. Bio-magnetostratigraphic correlation from Leg 107 in the Thyrrenian sea, in *Proc. ODP, Sci. Results.* Vol. **107,** 669–682, eds Kastens, K. A., Mascle, J. *et al.*

Channell, J. E. T., Rio, D. & Thunell, R. C., 1988. Miocene–Pliocene boundary magnetostratigraphy at Capo Spartivento, Calabria, Italy, *Geology,* **16,** 1096–1099.

Cita, M. B., 1975. The Miocene–Pleistocene boundary: history and definition, in *Late Neogene Epoch Boundaries,* Micropal., Spec. Publ. **1,** 1–30, eds Saito, T. & Burckle, L. H.,

Colalongo, M. L., Padovani, A., Sartoni, S., Tampieri, R., d'Onofrio, S., Elmi, C., Francavilla, F., Manzoni, M., Poluzzi, A. & Russo, A., 1972. Biostratigrafia e cronostratigrafia del Pliocene, *Boll. Soc. Geol. Ital.,* **93,** 489–509.

Colalongo, M. L. & Pasini, G., 1980. La Ostracofauna della sezione di Vrica in Calabria (con considerazioni sul limite Neogene/Quaternario). *Boll. Soc. Pal. Ital.,* **19** (1), 44–126.

Colalongo, M. L., Pasini, G., Pelosio, G., Raffi, S., Rio, D., Ruggieri, G., Sartoni, S., Selli, R. & Sprovieri, R., 1982. The Neogene/Quaternary boundary definition: a review and proposal, *Geogr. Fis. Dinam. Quartern.,* **5,** 59–68.

Colalongo, M. L., Pasini, G., Raffi, I., Rio, D., Sartoni, S. & Sprovieri, R., 1984. Biochronology of the Italian marine Pliocene and lower Pleistocene, Quarternary Geology and Geomorphology. *Geological Congress,* **3,** 109–127.

Colalongo, M. L., Pasini, G. & Sartoni, S., 1981. Remarks on the Neogene/Quaternary Boundary and the Vrica section (Calabria, Italy), *Boll. Soc. Paleontol Ital.,* **20,** 99–120.

Collinson, D. W., 1983. *Methods in Rock Magnetism and Palaeomagnetism,* Chapman and Hall, London.

Collombat, H., Rochette, P. & Kent, D. J., 1992. Possible correction of the inclination error in deep sea sediments using the anisotropy of anhysteretic remanence (ARM), *Bull. Soc. Géol. France,* (in press).

Dekkers, M. J., 1988. Magnetic properties of natural pyrrhotite. I: behaviour of initial susceptibility and saturation-magnetization-related rock-magnetic parameters in a grainsize dependent framework, *Phys. Earth planet. Interiors,* **52,** 376–393.

Dekkers, M. J., 1989. Magnetic properties of natural pyrrhotite. II: high- and low-temperature behaviour of Jrs and TRM as function of grain size, *Phys. Earth planet. Interiors,* **57,** 266–283.

Glaçon, G., Rio, D. & Sprovieri, R., 1990. Calcareous plankton Pliocene–Pleistocene biostratigraphy in the Tyrrhenian Sea (western Mediterranean, Leg 107), *Proceedings Ocean Drilling Program, Scientific Results,* Vol. **107,** 683–693.

Harland, W. B., Armstrong, R. L., Cox, A. V., Craig, L. E., Smith, A. G. & Smith, D. G., 1990. *A geological time scale* 1989, Cambridge University Press, Cambridge.

Herrero-Bervera, E. & Theyer, F., 1986. Non axisymetric behaviour of Olduvai and Jaramillo polarity transitions recorded in North-Central Pacific Deep-Sea Sediments, *Nature,* **322,** 159–164.

Hilgen, F. J. & Langereis, C. G., 1988. The age of the Miocene–Pliocene boundary in the Capo Rossello area (Sicily), *Earth planet. Sci. Lett.,* **91,** 214–222.

Hills, S. C. & Thierstein, H. R., 1989. Plio/Pleistocene calcareous plankton biochronology, in Special Issue 'Plankton Biochronology, Marine Micropaleontology' (eds. Haq, B. U.), *Mar. Micropaleontol.* **14**(1–3), 67–96.

Iaccarino, S., 1967. Les foraminifères du stratotype du Tabianien (Pliocène inférieur) de Tabiano Bagni (Parme), *Mem. Soc. Ital. Sci. Nat. Milano,* **15,** 165–180.

Iaccarino, S., 1985. Mediterranean Miocene and Pliocene planktic foraminifera, in *Plankton Stratigraphy,* pp. 283–314, eds Bolli, H. M., Saunders, J. B. & Perch-Nielsen, K., Cambridge University Press, Cambridge.

Iaccarino, S. & Papani, G., 1979. Il Messiniano dell'Appennino settentrionale dalla Val d'Arda alla Val Secchia: stratigrafia e rapporti col substrato e il Pliocene, pp. 15–46, *S. Venzo volume,* Grapiche Step, Parma.

Iaccarino, S. & Papani, G., 1982. Cenni generali sulla Formazione clastica continentale del Messiniano superiore dell'Emilia occidentale, con particolare riferimento alla Sezione del T. Stirone, in *Guida alla geologia del margine appenninico–padano,* pp. 137–140, eds Cremonini, G. & Ricci Lucchi, F., Guida Geol. Reg. S.G.I., Bologna.

Iaccarino, S. & Pugliese, N., 1988. Prime considerazioni sul passaggio Zancleano–Piacenziano nella serie del torrente Stirone (Emilia–Romagna), *Atti IV Simposio Ecol. Paleoec. Com. Bent.,* Sorrento, pp. 805–814.

Iaccarino, S., Capotondi, L., Mary, C., Turco, E. & Vergnaud Grazzini, C., 1993. *Biostratigraphy of the Pliocene Stirone Section* (in prep), Parma, Northern Italy.

Jenkins, D. G., 1987. Was the Pliocene–Pleistocene Boundary placed at the wrong level? *Quaternary Sci. Reviews,* **6,** 41–42.

King, J., Banerjee, S. K., Marvin, J. & Özdemir, O., 1982. A comparison of different magnetic methods for determining the relative grain size of magnetite in natural materials: some results from lake sediments, *Earth planet. Sci. Lett.* **52,** 404–419.

Kirschvink, J. L., 1980. The least-squares line and plane and the analysis of palaeomagnetic data, *Geophys. J. R. astr. Soc.,* **62,** 699–718.

Kukla, G., Collins, B. P. & Bender, M. L., 1979. Radiometric Age of the *Artica islandica Boundary in Italy*: 2 *My in VIIth Int. Congr. Mediterranean Neogene,* Ann. Geol. Pays Hellén., Tome hors-série, Fasc. 2, 699–709.

Laj, C., Jamet, M., Sorel, D. & Valente, J. P., 1982. First paleomagnetic results from Mio–Pliocene series of the Hellenic sedimentary Arc, *Tectonophysics,* **86,** 45–76.

Linssen, J. H., 1988. Preliminary results of a study of four successive sedimentary geomagnetic reversal records from the Mediterranean (Upper Thvera, Lower and Upper Sidufjall, and Lower Nunivak), *Phys. Earth planet. Interiors* **52,** 207–231.

Lovlie, R., Stole, G. & Spjeldnaes, N., 1989. Magnetic polarity stratigraphy of Pliocene–Pleistocene marine sediments from Rhodos, eastern Mediterranean, *Phys. Earth planet. Interiors* **54,** 340–352.

Mary, C., 1991. *Les inversions du champ magnétique terrestre: étude de la fidélité de deux enregistrements magnétostratigraphiques et représentation vectorielle du champ magnétique transitionnel.* Thèse de doctorot, Université Paris, **7,** 254 pp.

McElhinny, M. W., 1973. *Palaeomagnetism and plate tectonics,* Cambridge Earth Science Series, Cambridge University Press, Cambridge.

Morgan, G. E., 1979. Paleomagnetic results from DSDP site 398, in *Rep. Deep Sea Drill. Project* **47** 599–611.

Nakagawa, H., 1977. Magnetostratigraphy of the Pliocene–Pleistocene Boundary, *Giornale di Geologia,* **41,** 315–329.

Nicolas, A., 1989. *Structure of Ophiolites and Dynamics of Oceanic Lithosphere,* Kluwer Academic Publishers, Dordrecht.

Papani, G. & Pelosio, G., 1962. La serie Plio–Pleistocenica del T. Stirone (Parmense Occidentale), 2° Contributo alla conoscenza dei nuovi affioramenti fossiliferi del Calabriano nel Preappennino parmense, *Boll. Soc. Geol. Ital.,* **81,** 293–335.

Pasini, G., Colalongo, M. L. & Sartoni, S., 1992. Sedimentology, biostratigraphy, magnetostratigraphy, biochronology and radiometric dating of the Vrica Section in Calabria (Italy), in Van Couvering J. A., ed. *The Pliocene/Pleistocene boundary: definition and worldwide correlation,* (in press) Cambridge University Press, Cambridge.

Pelosio, G. & Raffi, S., 1973. Considerazioni sul limite Plio–Pleistocene nella serie del T. Crostolo (Preappennino Reggiano), *Ateneo Parmense, Acta Nat.,* **9,** 39–69.

Pelosio, G. & Raffi, S., 1977. *Preliminary remarks on mollusc assemblages of the Stirone River Pleistocene series,* Inst. Geology, Univ. Parma, Parma province, Northern Italy.

Pelosio, G., Raffi, S. & Rio, D., 1979. The Plio–Pleistocene boundary controversy. Status in 1979 at the light of International Stratigraphic Guide, *Sergio Venzo volume,* 131–140.

Raffi, S., 1982. Stato delle conoscenze sulla sezione pleistocenica marina del torrente Stirone (Parma), in *Guida alla geologia del margine appenninico–padano,* pp. 141–144, eds Cermonini, G. & Ricci Lucchi, F. Guida Geol. Reg. S.G.I., Bologna.

Raffi, S., 1986. The significance of marine boreal molluscs in the early Pleistocene faunas of the Mediterranean Area, *Palaeogeogr. Palaeoclimatol. Palaeoecol.,* **52,** 267–289.

Rio, D., Backman, J., Raffi, I., 1992. Calcareous nannofossil biochronology and the Pliocene/Pleistocene boundary, in *The Neogene/Quaternary Boundary,* Final Report of the I.G.C.P. Project n. 41, (in press).

Rio, D., Raffi, I. & Villa, G., 1990. Pliocene–Pleistocene calcareous nannofossil distribution patterns in the western Mediterranean. *Proceedings Ocean Drilling Program, Scientific Results,* Vol **107,** 513–533.

Rio, D., Sprovieri, R. & Raffi, I., 1984. Calcareous Plankton Biostratigraphy and Biochronology of the Pliocene–Lower

Pleistocene succession of the Capo Rossello Area, Sicily, *Mar. Micropaleontol.*, **9,** 135–180.

Rio, D., Sprovieri, R., Raffi, I. & Valleri, G., 1988. Biostratigrafia e paleoecologia della sezione stratotipica del Piacenziano, *Boll. Soc. Ital. Paleont.*, **27,** 213–238.

Rio, D., Sprovieri, R., Thunell, R., 1991. Pliocene–lower Pleistocene chronostratigraphy: A re-evaluation of Mediterranean type sections, *Geol. Soc. Am. Bull.*, **103,** 1049–1058.

Ryan, W. B. F. & Flood, J. D., 1973. Preliminary Paleomagnetic Measurements on Sediments from the Ionian (Site 125) and Tyrrhenian (Site 132) Basins of the Mediterranean sea, in. *Rep. D.S.D.P.*, Leg **13,** 599–603.

Schwarz, E. J. 1975. Magnetic properties of Pyrrhotite and use in applied Geology and Geophysics, *Geol. Surv. Can. Pap.*, 74–59, 24 pp.

Tauxe, L., Opdyke, N. D., Pasini, G. & Elmi, C., 1983. Age of the Plio–Pleistocene boundary in the Vrica section, Southern Italy, *Nature,* **304,** 125–129.

Tric, E., Laj, C., Jehanno, C., Valet, J. P., Kissel, C., Mazaud, A. & Iaccarino, S., 1991. High-resolution record of the upper Olduvai polarity Transition from Po Valley (Italy) sediments: support for dipolar transition geometry? *Phys. Earth planet. Interiors,* **65,** 319–336.

Zachariasse, W. J., Zijderveld, J. D. A., Langereis, C. G., Hilgen, F. J. & Verhallen, P. J. J. M., 1989. Early late Pliocene biochronology and surface water temperature variations in the Mediterranean, *Mar. Micropaleontol.*, **14,** 339–355.

Zijderveld, J. D. A., Zachariasse, J. W., Verhallen, P. J. J. M. & Hilgen, F. J., 1986. The age of the Miocene–Pliocene boundary, *Newsletter in Stratigraphy* **16,** 169–181.